

Article

Biogenic Nanoparticles Silver and Copper and Their Composites Derived from Marine Alga *Ulva lactuca*: Insight into the Characterizations, Antibacterial Activity, and Anti-Biofilm Formation

Ragaa A. Hamouda ^{1,2,*}, Mada A. Alharthi ¹, Amenah S. Alotaibi ³ , Asma Massad Alenzi ³, Doha A. Albalawi ³ and Rabab R. Makharita ^{1,4} 

¹ Department of Biology, College of Sciences and Arts Khulais, University of Jeddah, Jeddah 21959, Saudi Arabia

² Department of Microbial Biotechnology, Genetic Engineering and Biotechnology Research Institute, University of Sadat City, Sadat City 32897, Egypt

³ Genomic & Biotechnology Unit, Department of Biology, Faculty of Science, University of Tabuk, Tabuk 71491, Saudi Arabia

⁴ Botany and Microbiology Department, Faculty of Science, Suez Canal University, Ismailia 41522, Egypt

* Correspondence: rahamouda@uj.edu.sa or ragaahom@yahoo.com or ragaa.hamouda@gebri.usc.edu.eg

Abstract: Bacterial pathogens cause pain and death, add significantly to the expense of healthcare globally, and pose a serious concern in many aspects of daily life. Additionally, they raise significant issues in other industries, including pharmaceuticals, clothing, and food packaging. Due to their unique properties, a great deal of attention has been given to biogenic metal nanoparticles, nanocomposites, and their applications against pathogenic bacteria. This study is focused on biogenic silver and copper nanoparticles and their composites (UL/Ag₂ O-NPS, UI/CuO-NPs, and UI/Ag/Cu-NCMs) produced by the marine green alga *Ulva lactuca*. The characterization of biogenic nanoparticles UL/Ag₂ O-NPS and UI/CuO-NPs and their composites UI/Ag/Cu-NCMs has been accomplished by FT-IR, SEM, TEM, EDS, XRD, and the zeta potential. Minimum inhibitory concentration (MIC) and minimum bactericidal concentration (MBC) experiments were conducted to prove antibacterial activity against both Gram-positive and Gram-negative bacteria and anti-biofilm. The FTIR spectroscopy results indicate the exiting band at 1633 cm⁻¹, which represents N–H stretching in nanocomposites, with a small shift in both copper and silver nanoparticles, which is responsible for the bio-reduction of nanoparticles. The TEM image reveals that the UI/Ag/Cu-NCMs were hexagonal, and the size distribution ranged from 10 to 35 nm. Meanwhile, UI/CuO-NPs are rod-shaped, whereas UL/Ag₂ O-NPS are spherical. The EDX analysis shows that Cu metal was present in a high weight percentage over Ag in the case of bio-Ag/Cu-NCMs. The X-ray diffraction denotes that UI/Ag/Cu-NCMs, UL/CuO-NPs, and UL/Ag₂ O-NPS were crystalline. The results predicted by the zeta potential demonstrate that UI/Ag/Cu-NCMs were more stable than UI/CuO-NPs. The antibacterial activity of UL/Ag₂ O-NPS, UI/Ag/Cu-NCMs, and UL/CuO-NPs was studied against eleven Gram-negative and Gram-positive multidrug-resistant bacterial species. The maximum inhibition zones were obtained with UL/Ag₂ O-NPS, followed by UI/Ag/Cu-NCMs and UI/CuO-NPs in all the tested bacteria. The maximum anti-biofilm percentage formed by *E. coli* KY856933 was obtained with UL/Ag₂ O-NPS. These findings suggest that the synthesized nanoparticles might be a great alternative for use as an antibacterial agent against different multidrug-resistant bacterial strains.

Keywords: *Ulva lactuca*; Ag nanoparticles; copper nanoparticles; nanocomposites; antibacterial



Citation: Hamouda, R.A.; Alharthi, M.A.; Alotaibi, A.S.; Alenzi, A.M.; Albalawi, D.A.; Makharita, R.R. Biogenic Nanoparticles Silver and Copper and Their Composites Derived from Marine Alga *Ulva lactuca*: Insight into the Characterizations, Antibacterial Activity, and Anti-Biofilm Formation. *Molecules* **2023**, *28*, 6324. <https://doi.org/10.3390/molecules28176324>

Academic Editor: Keykavous Parang

Received: 24 July 2023

Revised: 23 August 2023

Accepted: 25 August 2023

Published: 29 August 2023



Copyright: © 2023 by the authors. Licensee MDPI, Basel, Switzerland. This article is an open access article distributed under the terms and conditions of the Creative Commons Attribution (CC BY) license (<https://creativecommons.org/licenses/by/4.0/>).

1. Introduction

Nanotechnology, in combination with biology, provides a promising field of nanobiotechnology. This includes living entities, such as cyanobacteria, bacteria, viruses, algae, acti-

nomycetes, yeasts, fungi, and plants [1–3]. The green biogenesis of nanoparticles (NPs) utilizing either algae or plant extracts has appeared to be an economical and environmentally beneficial technique [4–6]. Specifically, macro-algae cover various bioactive contents with multiple constructions and promising biological applications [7,8]. Due to their potential utility in the bio-manufacture of nanomaterials, algae have been referred to as “nanofactories”. The main benefit of this environmentally friendly fabrication is the lack of hazardous solvents and reagents, which prevents the production of waste and byproducts during the synthesis of metal nanoparticles. In addition, the use of algae fosters the goal of using natural, renewable resources [9,10]. The process of metal stabilization and reduction is supported by a variety of substances found in the crude extracts of macroalgae, such as amines, amides, alkaloids, terpenoids, pigments, proteins, etc. [11,12]. *Ulva lactuca* is a type of green seaweed comprised of highly active substances with antitumor, antioxidant, hypocholesterolemic, and antimicrobial capabilities [13]. Ag-NPs can be fabricated using *U. lactuca* [14]. Ag-NPs fabricated using *U. lactuca* have antibacterial activities against *Escherichia coli* and *Pseudomonas aeruginosa* [15]. The biosynthesis of nanoparticles by *U. lactuca* is a reliable, economical, and eco-friendly process for the synthesis of metallic nanoparticles [16].

A nanocomposite is a composite material in which at least one of the materials is one dimension in size, around 10–9 nm [17]. They have high-performance materials that exhibit rare characteristics. Their perspective is so notable that they are valuable in many fields [18], from packaging to biomedical applications [19]. The antifungal effect resulting from the copper–silver–chitosan nanocomposite was more significant than that of other nanoparticles tested, which has had an essential influence on the growth of *Candida albicans* in laboratory conditions compared to other nanoparticles [20]. Different studies showed that the as-synthesized Ag/Cu-NMCs could be an efficient substitute for an antimicrobial agent against drug-resistant microbes and plant-pathogenic bacteria [21,22]. The Ag–Cu–Co oxide caused a maximum zone of inhibition against *E. coli* that was found to be 25 mm [23]. The fabricated nanostructured surfaces (Ag–Cu_xO nanostructures) exhibit excellent bactericidal efficiency against *E. coli* (Gram-negative) and *Staphylococcus aureus* (Gram-positive) [24]. Good antibacterial activity was noted against both bacteria in milk (*Escherichia coli* and *Staphylococcus aureus*) with a sensitivity of 40–90% at CuO/Ag concentrations ranging from 6 to 200 mg/100 mL [25]. CuO/Ag₂O NCPs synthesized by the leaf extract of *Eichhornia crassipes* show good antibacterial activities against four human pathogenic bacteria, such as *K. pneumoniae*, *E. coli*, *S. epidermidis*, and *S. aureus* [26].

Due to their unique characteristics, such as superior electrical conductivity, low electrochemical migration behavior, a high melting point, and, most importantly, low cost, copper nanoparticles have applications in many areas, such as industries, medicine, electronics, etc. [27,28]. For more than 200 years, copper has been known for its ability to inhibit the growth of microorganisms and lower microbial concentrations by 99.9% [29,30]. Numerous studies have shown that copper nanoparticles show excellent antimicrobial activity against many bacteria [28,31]. Moreover, nano-copper oxide (Cu–O) works as an essential antimicrobial agent against *Staphylococcus aureus*, *Escherichia coli*, *Vibrio cholera*, *Pseudomonas aeruginosa*, *Bacillus subtilis*, and *Syphillis typhus* [32–35]. The reputation of copper has expanded lately with the COVID-19 pandemic, when it was noticed that SARS-CoV-2 on copper surfaces decomposes more rapidly (in four hours) than other materials, such as plastic and stainless steel [36].

This study aims to investigate the efficacy of the marine green alga *Ulva lactuca*, collected from the Jeddah seashore, as reducing and stabilizing agents for the biofabrication of UL/Ag₂O-NPS, UL/CuO-NPs, and UL/Ag/Cu-NMCs. We have compared the characteristics of silver and copper nanoparticles and their composites. We have also determined the antibacterial activities of biofabricated nanoparticles and their composites against some multi-drug-resistance bacterial strains.

2. Results and Discussion

2.1. Characterisation of UI/Ag₂O-NPS, UI/Ag/Cu-NCMs, and UI/CuO-NPs

2.1.1. Fourier Transform Infrared (FTIR) of UL/Ag₂O-NPS, UI/Ag/Cu-NCMs and UI/CuO-NPs

Fourier transform infrared spectroscopy was conducted to reveal the functional groups in the molecules characterized during the production of the newly synthesized nanoparticles, which are responsible for the stabilization and coating of the nanoparticles in all three nanoparticles. The FTIR spectra bands of the silver nanoparticles are shown in Figure 1 and Table 1. The silver nanoparticles (UL/Ag₂O-NPS) biofabricated by *U. lactuca* illustrate 10 peaks at 3752, 3419, 2426, 1765, 1636, 1383, 1202, 1097, 826, and 606 cm⁻¹. The FT-IR spectroscopy of the UI/CuO-NPs shows 17 peaks at 3587, 3564, 3390, 2927, 1635, 1386, 1123, 1090, 988, 944, 876, 781, 724, 623, 601, 483, and 420 cm⁻¹. The silver/copper nanocomposites exhibit 18 peaks at 3588, 3565, 3390, 2925, 1633, 1125, 1088, 1025, 987, 944, 874, 780, 733, 631, 600, 509, 483 and 417 cm⁻¹. The band at 1633 cm⁻¹, which is present in all of the synthesized nanoparticles (UL/Ag₂O-NPS, UI/Ag/Cu-NCMs, and UI/CuO-NPs) with a small shift, represents the N–H stretching band, which denotes the active group that acts as reducing and stabilizing agents in biofabricated nanoparticles. Phytochemical compounds found in biomass, such as alcohols, aldehydes, alkanes, and epoxy groups or ether groups, can be responsible for the nucleation process to reduce Ag⁺ to Ag⁰ [37]. The biosynthesis of nanoparticles may be triggered by several compounds, such as carbonyl groups, phenolics, flavonones, terpenoids, amides, amines, proteins, pigments, alkaloids, and other reducing agents present in the biological extracts [11].

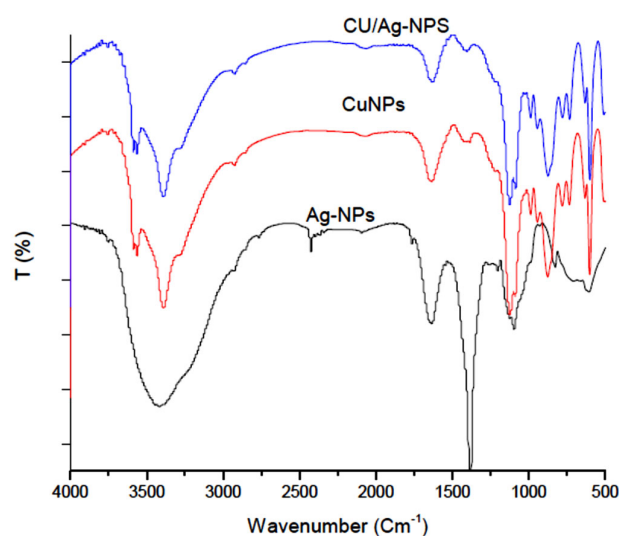


Figure 1. Fourier transform infrared spectroscopic data of UI/Ag₂O-NPS, UI/Ag/Cu-NCMs, and UI/CuO-NPs derived from *U. lactuca*.

Table 1. Absorption peaks assigned to the active groups of UI/Ag₂O-NPS, UI/Ag/Cu-NCMs, and UI/CuO-NPs derived from *U. lactuca*.

Wavenumber cm ⁻¹	UI/Ag/Cu-NCMs	UI/CuO-NPs	UL/Ag ₂ O-NPS	Assignment	References
3752	Nd	Nd	D	OH bonds	[38]
3588	D	–1	Nd	OH bonds	[39]
3565	D	–1	Nd	OH bonds	[40]
3419	Nd	Nd	D	Bonded N–H/C–H/O–H stretching of amines and amides	[41]
3390	D	D	Nd	O–H Stretching	[42]

Table 1. Cont.

Wavenumber cm^{-1}	UI/Ag/Cu-NCMs	UI/CuO-NPs	UL/Ag ₂ O-NPS	Assignment	References
2925	D	+2	Nd	CH stretching bands	[43]
2426	Nd	Nd	D	Carboxyl acid	[41]
1765	Nd	Nd	D	Carbonyl stretching C=O	[44]
1633	D	+2	+3	N-H stretching band	[45]
1386	Nd	D	-3	C-H stretching	[46]
1202	Nd	Nd	D	Alkyl amine	[47]
1125	D	-2	Nd	Amide III band region	[48]
1088	D	+2	-9	C-N stretching absorption of primary aliphatic amines	[49]
1025	D	Nd	Nd	Aromatic C-H in plane deformation	[50]
987	D	+1	Nd	Si-O stretching region	[51]
944	D	D	Nd	Phosphodiester region	[51]
874	D	+2	Nd	Organosulfate C-O-S	[52]
826	Nd	Nd	D	Stretching, C-C	[41]
780	D	+1	Nd	Pyridine (pyridine ring vibration and C-H deformation)	[53]
733	D	+1	Nd	Cu-O	[54]
631	D	+1	Nd	OH Stretching	[55]
600	D	+1	+6	Ring deformation of phenyl	[54]
509	D	Nd	Nd	Cu-O	[56]
483	D	D	Nd	Cu-O	[56]
417	D	+3	Nd	Cu-O	[56]

D: Detected; Nd: Not Detected; (-): shifted wavenumber by minus; (+): shifted wavenumber by addition.

2.1.2. Scanning and Transmission Electron Microscope (SEM and TEM) of UL/Ag₂ O-NPS, UI/CuO-NPs, and UI/Ag/Cu-NCMs Derived from *U. lactuca*

The SEM image has been used to illustrate the size and shape of the produced nanoparticles. As shown in the sample images in Figure 2A–C, the surface is rough due to the presence of Cu, Ag, and Ag combined with Cu. The modification in morphology and coarseness of the surface was due to the foundation of nanoparticles [57].

The TEM image shows that UL/Ag₂O-NPS are spherical in shape and range from 10 to 45 nm (Figure 2D and Table 2). The image proves that UL/Ag₂ O-NPS are polydispersed and range in size from 15 to 20 nm, as shown in the frequency histogram (Figure 2G). The Ag-NPs synthesized by *Ulva fasciata* were spherical and 50 nm in size [58]; by *Enteromorpha flexuosa* were 2–32 nm/circular [59]; by *Padina tetrastromatica* were 14 nm/spherical [60]; and by *Gracilaria corticata* were 8–46 nm/spherical [61].

The TEM image of the UI/CuO-NPs shows they are rod-shaped, one-dimensional nanoparticles; the length of the rod ranged from 46 to 65 nm, and the width ranged from 10 to 40 nm (Figure 2E). The UI/CuO-NPs are polydispersed and range in size, according to width, from 20 to 25 nm (Figure 2E and Table 2). The size of the synthesized copper nanoparticles using *Zingiber officinale* and *Curcuma longa* rhizome extract was in the nano-range of approximately 20 to 100 nm [62], and the average size of the copper nanoparticles synthesized by *Eucalyptus* leaf extract ranged from 10 to 130 nm. In contrast, the size of the mint leaf extracts of the copper nanoparticles ranged from 23 to 39 nm [63]. The results estimated that there was some aggregation of UI/CuO-NPs; some nanoparticles were well distributed, while most were found in the agglomerated form [63]. The results agree with Ramzan et al. [64] when using *Cedrus deodara* aqueous extract to synthesize the copper nanoparticles; only a few spherical-shaped and well-separated particles were found, and most of them were agglomerated. Amaliyah et al. [65] used *Piper retrofractum* Vahl extract to synthesize spherical Cu-NPs with the propensity to form a random aggregate. Moreover, Mahmoud et al. [66] utilized orange peels to synthesize CuO-NPs, which appear to aggregate. Meanwhile, when Ag and Cu were loaded to form UI/Ag/Cu-NCMs, the shape and size changed to a hexagonal shape, and they were well distributed in the

solution with a size range of 10–35 nm (Figure 2G and Table 2). The image denotes polydispersed UI/Ag/Cu-NCMs with a frequency in the range of 15 to 20 nm with 39%. The image demonstrates there is a core shell around the UL/Ag₂ O-NPS, UI/CuO-NPs, and UI/Ag/Cu-NCMs; the shell appears faint and dark around the nanoparticles and is denoted by arrows in the images. The shell may be related to organic compounds derived from *U. lactuca*.

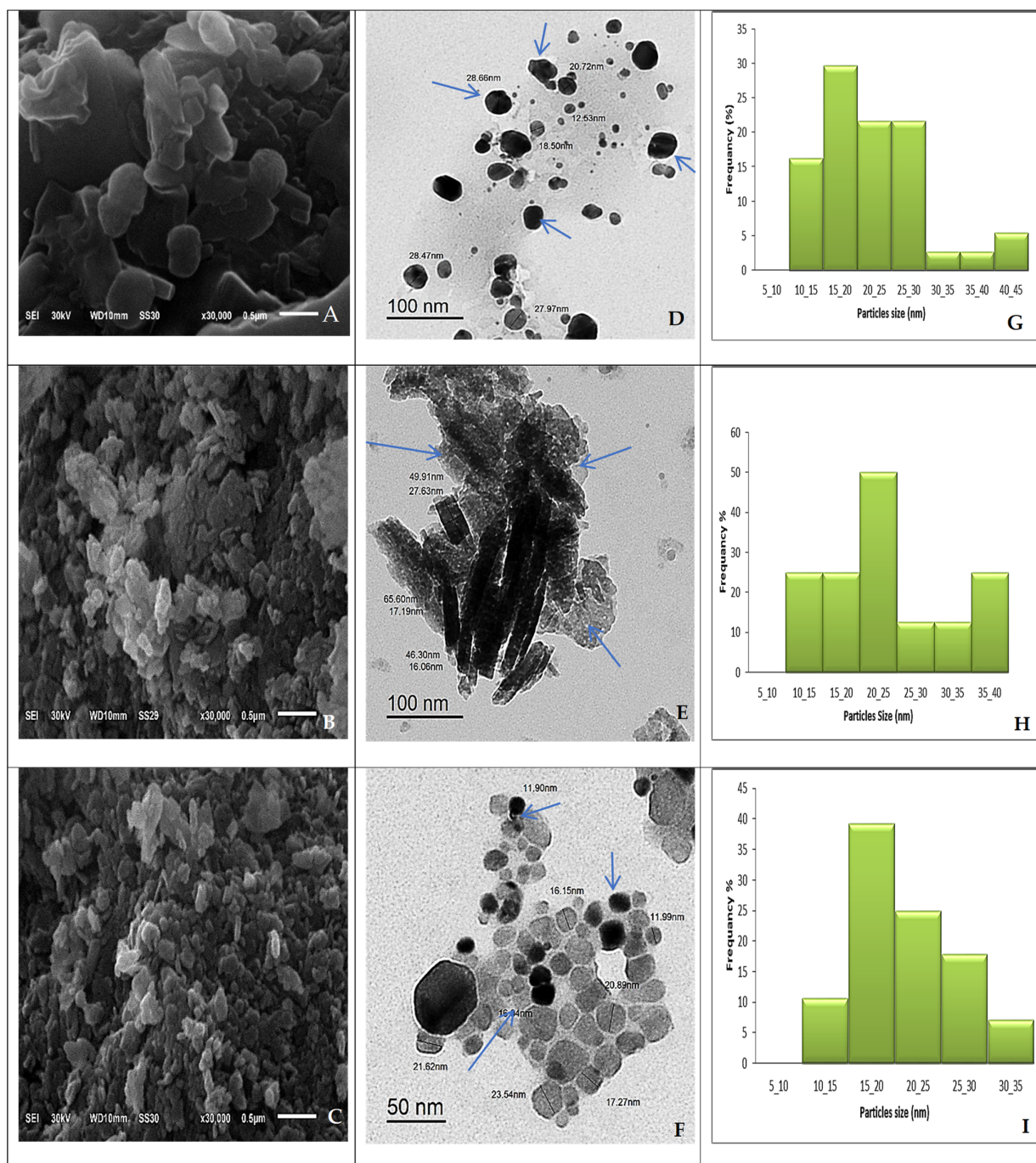


Figure 2. The SEM (A–C) and TEM (D–F) images and frequency distribution (%) (G–I) of UL/Ag₂ O-NPS, UI/CuO-NPs, UI/Ag/Cu-NCMs derived from *U. lactuca*. Arrows refer to the shell around nanoparticles.

Table 2. The main differences between biofabricated nanoparticles by *U. lactuca*.

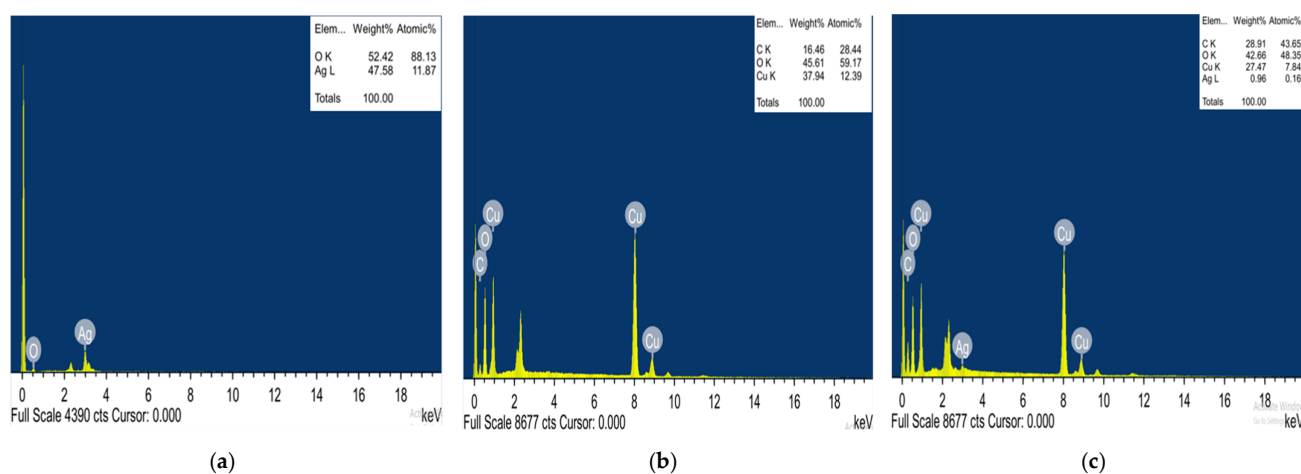
Biofabricated Nanoparticles	Shape	Size Range (nm)	Size Range (nm) (Predominant)	Frequency%
UL/Ag ₂ O-NPS	Spherical	10–45	15–20	28%
UI/CuO-NPs	Rod	10–40	20–25	50%
UI/Ag/Cu-NCMs	Hexagonal	10–35	15–20	39%

The core-shell nanomaterials can be extended to the class of nanomaterials having distinct boundary materials covering (either fully or partially) the inner component. Core-shell nanoparticles (core-shell NPs) are structures that frequently combine the characteristics of the two (or more) materials used, with the shell controlling the surface properties of the particles while encasing the core entirely [67].

The results indicate that *U. lactuca* is an excellent reducing and stabilizing agent. López-Ubaldo et al. [68] reported the size of Ag/Cu-NCMs biosynthesized by *Ricinus communis* was in the range of 10–25 nm and spheroid in shape. The size of Ag/Cu-NCMs green synthesized by *Opuntia ficusindica*, as indicated by Rocha-Rocha et al. [69], ranged from 10 nm to 20 nm. Mohamad et al. [70] stated that leaf palm extract efficiently reduced and stabilized agents for the biosynthesis of Cu/Ag-Nano composites. The supernatant of *Rhodospseudomonas capsulate* showed high efficiency when it was used to synthesize Cu/Ag-NCMs.

2.1.3. Energy Dispersive X-ray (EDX) of UL/Ag₂O-NPS, UI/CuO-NPs, and UI/Ag/Cu-NCMs Derived from *U. lactuca*

Energy dispersive X-ray (EDX) is a vital analytical procedure used to verify the sample's elemental composition. Ag and O were found, by weight, in UL/Ag₂O-NPS at 54.42 and 47.58%, respectively. The chemical composition of the prepared UI/CuO-NPs was identified by EDX analysis, as shown in Figure 3b. The EDX analysis of the UI/CuO-NPs revealed that there was 37.94% copper, 45.61% oxygen, and 16.46% carbon. The four peaks are C, O, Cu, and Ag, with weight percentages of 28.91, 42.66, 27.47 and 0.96, respectively in UI/Ag/Cu-NCMs. The extensive presence of Cu over Ag may be related to the methods of synthesis that use 1:9 Ag:Cu in the synthesis of nanocomposites. The appearance of different elements, such as oxygen 42.66% and carbon 17.08%, may be due to the organic compounds found in the alga extract [71].

**Figure 3.** Energy dispersive X-ray (EDX) of UL/Ag₂O-NPS (a), UI/CuO-NPs (b), and UI/Ag/Cu-NCMs (c) derived from *U. lactuca*.

2.1.4. X-ray Diffraction (XRD) of UI/Ag₂ O-NPS, UI/CuO-NPs, and UI/Ag/Cu-NCMs Derived from *U. lactuca*

X-ray diffraction was used to investigate the size and crystallization of UL/Ag₂ O-NPS synthesized by *U. lactuca*. The results revealed the peak positions with 2θ values of 19.843, 29.841, 31.972, and 40.6. The Miller indices (h k l) for each peak were indexed as 100, 110, 110, and 111, respectively (Figure 4a, and Table 3a). These results confirm the formation of UL/Ag₂ O-NPS as nanocrystals, and the crystal size ranged from 12.2 to 36.7. The major crystalline peak was obtained at 2θ 29.841 with an intensity of 100% and a size of 12.2 nm. The X-ray diffraction of the Ag-NPs biofabricated by *Turbinaria urbinata* showed two intense peaks at 27.94 and 32.27, which correspond to Miller indices of 110 and 111 [72]. Five peaks of X-ray diffraction patterns were obtained with biofabricated Ag-NPs obtained by marine green alga *Ulva fasciata*, with 2θ values of 27.925, 32.409, 46.333, 57.582, and 76.618 degrees corresponding to 111, 200, 220, 222, and 331, respectively [73]. The X-ray diffraction peaks of gelatin-capped Ag-NPs biofabricated by *Oscillatoria limnetica* extract had 2θ values of 14.26, 24.15, 30.08, 32.02, and 42.01°, which correspond with Miller indices of 100, 100, 110, 110, and 111, respectively [74].

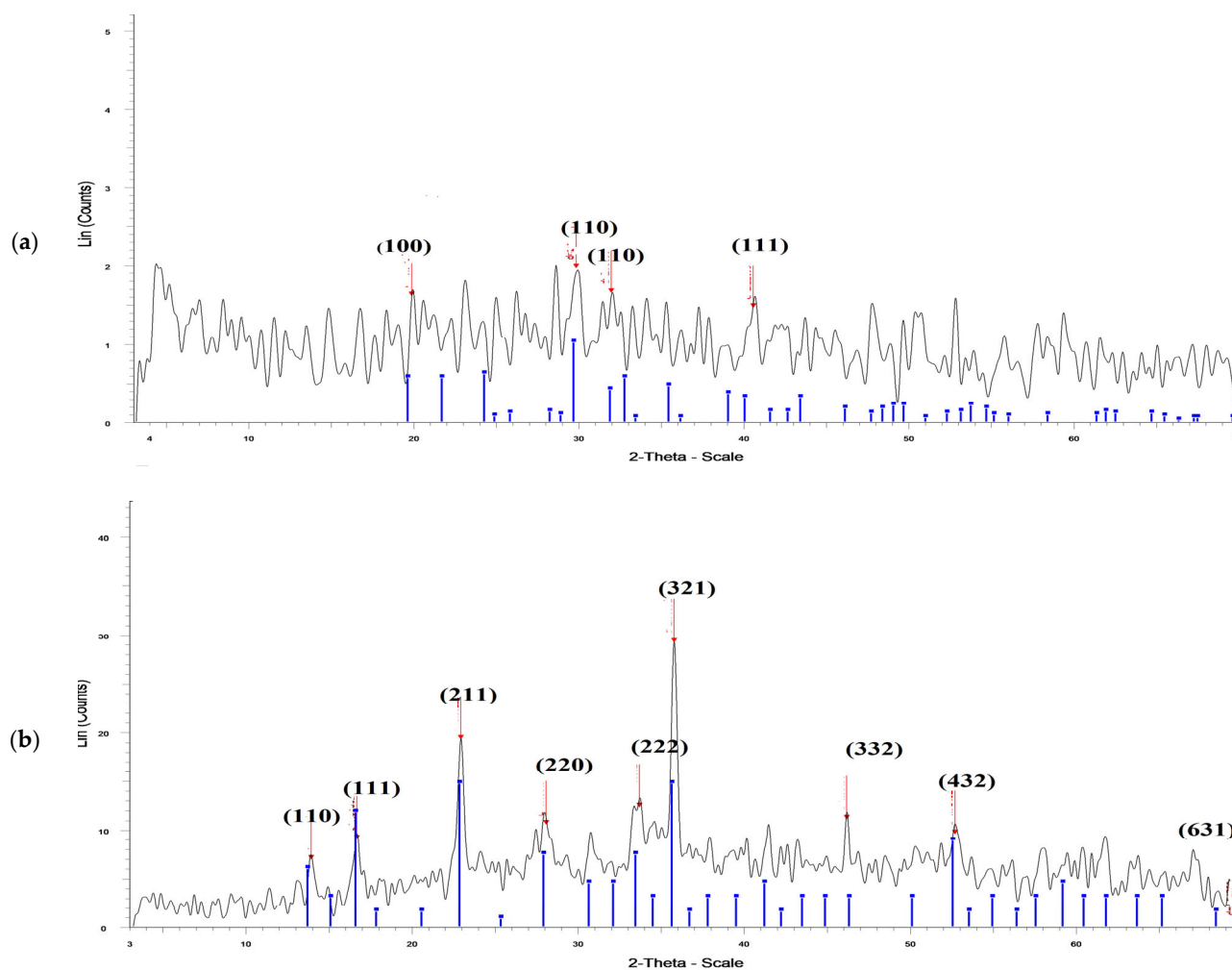


Figure 4. Cont.

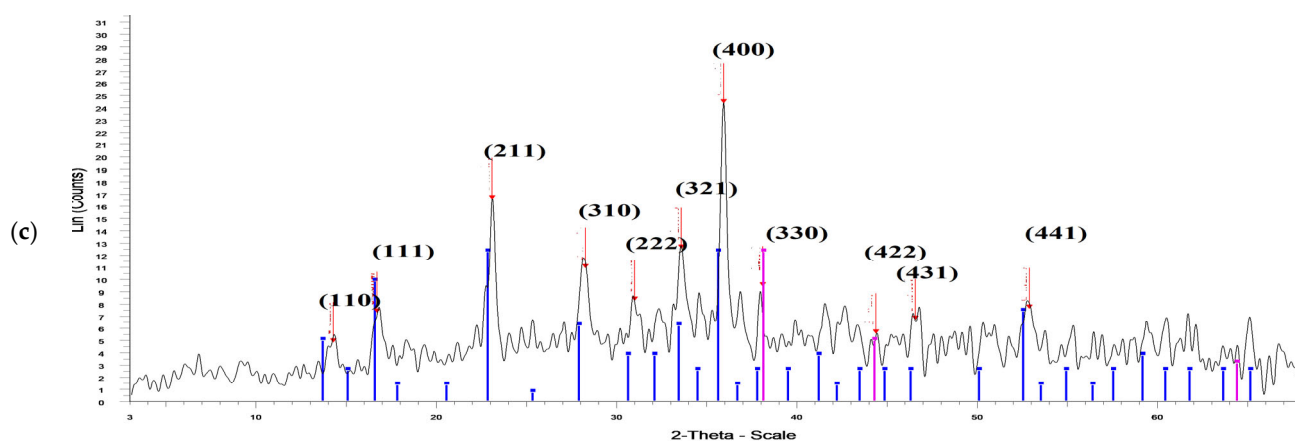


Figure 4. X-ray diffraction of UL/Ag₂O-NPS (a), UI/CuO-NPs(b), and UI/Ag/Cu-NCMs (c) derived from *U. lactuca*.

Table 3. (a) X-ray diffraction of UI/Ag₂O-NPS derived from *U. lactuca*. (b) X-ray diffraction of UI/CuO-NPs derived from *U. lactuca*. (c) X-ray diffraction of UI/Ag/Cu-NCMs derived from *U. lactuca*.

(a)					
Peak position 2 θ	$1000 \times \sin^2\theta$	$1000 \times \sin^2\theta/36$	Reflection	Crystal size (nm)	Intensity %
19.843	30	1	100	36.7	81.8
29.841	66	2	110	12.2	100
31.972	76	2	110	21.8	83.8
40.6	120	3	111	28.3	74.3
(b)					
13.865	15	2	110	24.1	23.7
16.608	22	3	111	20.9	30.8
22.889	40	6	211	28.4	66
28.035	59	8	220	0.7	36.1
33.673	85	12	222	8.2	42.1
35.763	95	14	321	21.3	100
46.167	153	22	332	14.7	38
52.718	199	29	432	10.5	32.7
69.226	327	46	631	33	0.9
(c)					
14.221	15	2	110	20.2	19.6
16.659	21	3	111	20	29.8
23.054	40	6	211	24.1	68.1
28.238	59	10	310	24.2	44.7
30.981	71	12	222	33.5	33.9
33.571	83	17	321	18.3	51.5
35.914	95	16	400	28.8	100
38.091	106	18	330	117.4	38.6
44.389	143	24	422	16.1	22.7
46.573	156	26	431	38.1	27.4
52.921	198	33	441	0.3	31.2

The XRD spectra of UI/CuO-NMPs derived from *U. lactuca* reveal the crystal lattice structure of the biosynthesized UI/CuO-NPs (Figure 4b and Table 3b). The XRD spectrum analysis for UI/CuO-NPs shows diffraction peaks at 2θ 13.865, 16.608, 22.889, 28.035, 33.673, 35.763, 46.167, 52.718, and 69.226; these diffraction peaks were indexed as 110, 111, 211, 220, 222, 321, 332, 432, and 631, respectively. The results demonstrate that the UI/CuO-NPs is crystalline, and the crystal size ranged from 8.2 to 33. The major crystalline peak was obtained at 2 theta 35.763 with an intensity of 100%, and a size of 21.3 nm. The peak positions of UI/CuO-NPS synthesized by macro green alga *Ulva fasciata* were at 2θ values of 16.36, 22.62, 27.77, 31.74, 35.43, 41.14, 52.37, 56.07, 60.02, 66.55, and 73.64, which were indexed as 100, 110, 111, 200, 320, 210, 211, 221, 310, 311, 222, and 320, respectively [57]. The diffraction peaks of Cu-NPs synthesized by red alga *Pterocladia capillacea* were at 2θ 10.9, 27.1, 31.5, 45.2, 56.3, and 75.1°, and were indexed (h k l) as 135, 114, 375, 220, and 105, respectively [75]. The XRD patterns of the Cu-NPs biofabricated by a soluble polysaccharide extracted from marine alga *Sargassum vulgare* were at 2θ 33.8, 39.7, 47.3, 65.7, and 78.8° indexed with Miller plans as 110, 111, 200, 220, and 313, respectively [76]. The results in Figure 4c and Table 3b show the peak positions of the XRD patterns of UI/Ag/Cu-NCMs derived from *U. lactuca*, with 2θ values of 14.22, 16.65, 23.05, 28.23, 30.98, 33.57, 35.91, 38.09, 44.38, 46.57, and 52.92; the Miller indices (h k l) for each peak were indexed as 110, 111, 211, 310, 222, 321, 400, 330, 422, 431, and 441, respectively. The most intense 100% peak was obtained at 2 theta 35.914 and size 28.8. The results denote the crystalline UL/Ag₂ O-NPS, UI/CuO-NPs, and UI/Ag/Cu-NCMs derived from *U. lactuca*.

2.1.5. Zeta Potential of UL/Ag₂ O-NPS, UI/CuO-NPs, and UI/Ag/Cu-NCMs Derived from *U. lactuca*

The zeta potential is an analysis method that measures the number of electric charges on the nanoparticle's surface. Figure 5 demonstrates the zeta potential of UL/Ag₂ O-NPS, UI/CuO-NPs, and UI/Ag/Cu-NCMs derived from *U. lactuca*. The results show that the zeta potential value of UL/Ag₂ O-NPS has a positive charge (+1.14), while the zeta potential values of UI/CuO-NPs and UI/Ag/Cu-NCMs have negative charges (−0.195 and −3.69, respectively). The zeta potential values differ according to the methods used and plant synthesis. The silver nanoparticles formed by the fungus *Trichoderma viride* had a positive charge [77]. The zeta potential values of the Ag-NPs produced by photosynthesis by *Oscillatoria limnetica* had a highly positive charge [78].

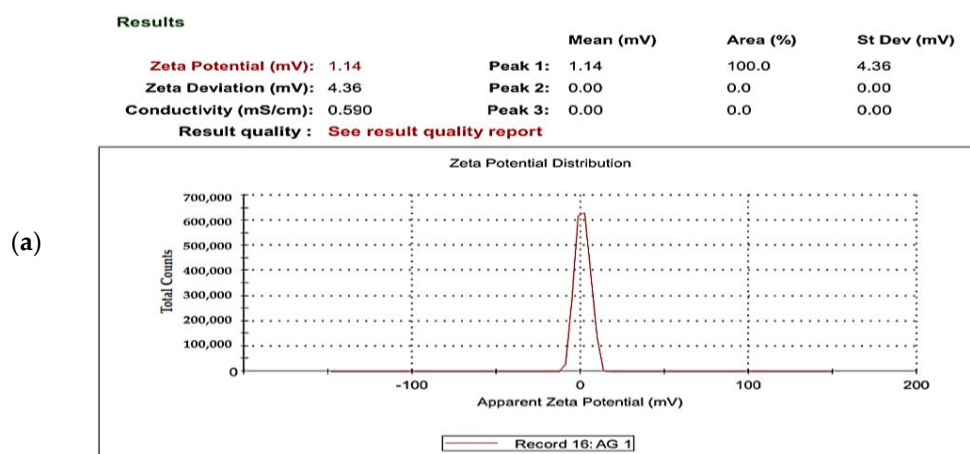


Figure 5. Cont.

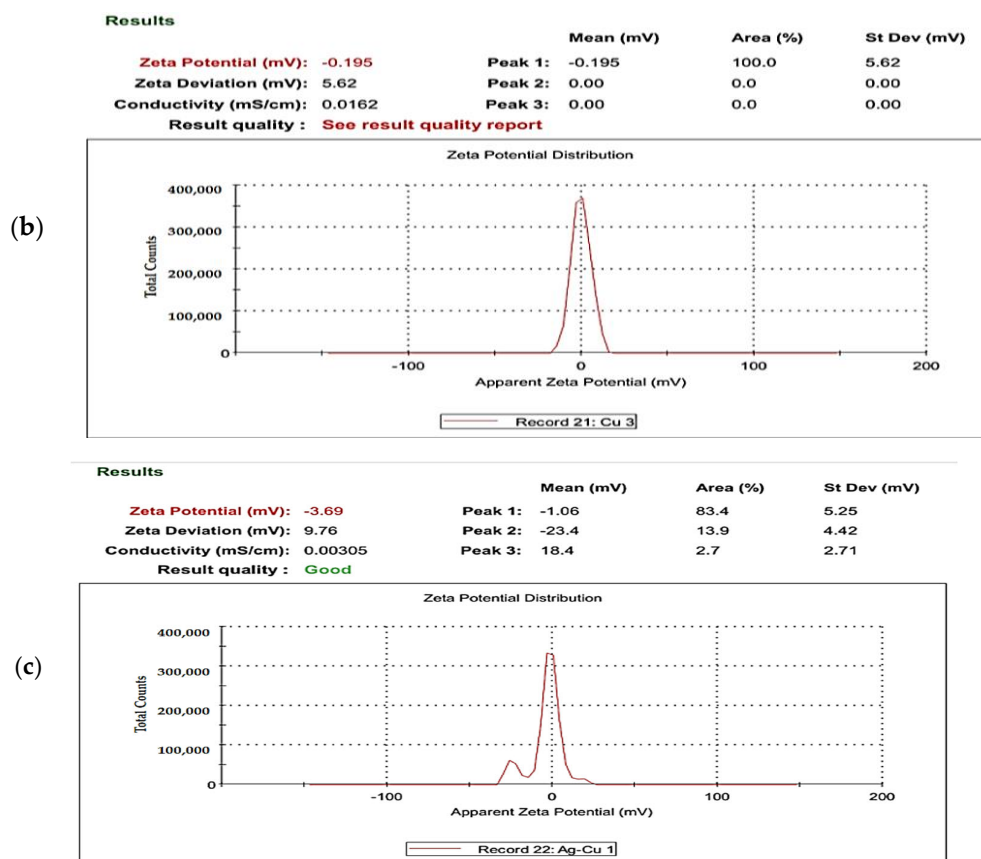


Figure 5. Zeta potential of UL/Ag₂ O-NPS (a), UI/CuO-NPs (b), and UI/Ag/Cu-NCMs (c) derived from *U. lactuca*.

2.2. Antibacterial Activity of Synthesized UL/Ag₂ O-NPS, UI/CuO-NPs, and UI/Ag/Cu-NCMs Derived from *U. lactuca*

The antibacterial activity of UL/Ag₂ O-NPS, UI/CuO-NPs, and UI/Ag/Cu-NCMs derived from *U. lactuca* in different volumes (10, 30, and 100 μ L at the same concentration of 1 mg/mL) was tested against 11 bacterial strains of Gram-negative and Gram-positive multidrug-resistant bacteria: *Streptococcus mutans* ATCC 25175 and *Lactobacillus acidophilus* CH-2 [79]. The results indicate that the different volumes and types of nanoparticles had significant effects on the antibacterial activity. The higher volumes (100 μ L/well) possessed higher antibacterial activities than 30 and 10 μ L/well (Figure 6 and Table 4). The maximum zone of inhibition for the volume (100 μ L) of UL/Ag₂ O-NPs was recorded against *Streptococcus mutans* ATCC 25175 (17 mm), followed by UI/Ag/Cu-NCMs (14 mm). No significant effect of UI/CuO-NPs (100 μ L) and UI/Ag-NPs with volume of 10 and 30 μ L were noted. The lowest inhibition zone was recorded with UI/CuO-NPs (10 and 30 μ L). The UL/Ag₂ O-NPS showed the highest antibacterial activity (18.3 mm at 100 μ L) against *Lactobacillus acidophilus* CH-2, followed by UI/Ag/Cu-NCMs (16 mm at 100 μ L). The UI/CuO-NPs showed the lowest antibacterial activity against *Staphylococcus aureus* ATCC6538 and *Staphylococcus aureus* in the inhibition zone (7 mm at 10, and 30 μ L). The UI/Ag-NPs and UI/Cu-NPs possessed better antibacterial activity against *Staphylococcus aureus* than the UI/Ag/Cu-NCMs with a volume of 100 μ L. The UL/Ag₂ O-NPs denoted the highest antibacterial activity against *Klebsiella pneumoniae* KY856924, *Acinetobacter* KY856930, *E. coli* KY856933, and *Enterobacter* KY856934 at 100 μ L/well, but the results showed that the UI/CuO-NPs had the highest antibacterial activity against *E. coli* KY856932, and UI/Ag/Cu-NCMs had higher activity against *Enterobacter aerogenes* at 100 μ L/well. This study demonstrates that the UL/Ag₂ O-NPS had more antibacterial activity in most tested bacteria, except *E. coli* KY856932 and *Enterobacter aerogenes*. The higher antibacterial activity of UL/Ag₂ O-NPS

over UI/CuO-NPs and UI/Ag/Cu-NCMs may be due to UI/Ag₂ O-NPs having a positive charge. The positively charged Ag-NPs displayed the largest inhibitory zones against all the strains tested and in all the concentrations employed. In any concentration examined, neutral and negatively charged AgNPs did not exhibit enough antibacterial action against *P. vulgaris* [80]. The positively charged BPEI-AgNPs were the most toxic NPs, whereas the more negatively charged citrate-AgNPs were the least hazardous [81]. Bacteria with a negative surface charge come into contact with nanoparticles with a positive zeta potential, and the electrostatic forces that result encourage a stronger attraction and interaction between the two organisms and may even allow for bacterial membrane penetration [82]. Also possible are the low-release UI/CuO-NPs and UI/Ag/Cu-NCMs. The Cu-NPs may possess antibacterial activity by denaturing the proteins and enzymes of bacteria [83]. An investigation was conducted by Chandraker et al. [84] and an excellent result was seen with a 12.43 mm zone of inhibition for the antibacterial activity of green Cu-NPs produced utilizing an aqueous leaf extract of *Ageratum houstonianum* against the Gram-negative bacterium *Escherichia coli*. A strong antibacterial effect of Cu-NPs on Gram-positive *Bacillus subtilis* and Gram-negative *Escherichia coli* was also mediated by an aqueous extract of *Curcuma longa*. When compared to Gram-positive bacteria, the Gram-negative bacteria had a greater zone of inhibitory growth, which suggests that the Gram-positive bacteria are more sensitive to Cu-NPs [85]. A previous study performed by Jayandran et al. [86] compared the antibacterial activities of Cu-NPs synthesized using curcumin against two Gram-positive (*Staphylococcus aureus* and *Bacillus subtilis*) and Gram-negative (*Escherichia coli*) bacteria to the antibacterial activity of pure curcumin. Fascinatingly, the zone of inhibition recognized for Cu-NPs against *S. aureus* and *B. subtilis* showed higher antibacterial activity than the normal drug, chloramphenicol.

Table 4. Effect of different volumes (10, 30, 100 µL) of UL/Ag₂ O-NPS, UI/CuO-NPs, and UI/Ag/Cu-NCMs (conc., 1 mg/mL) derived by *U. lactuca* in Gram-positive and Gram-negative bacteria, determined by inhibition zone (mm).

Bacterial Strains	Volume	UL/Ag ₂ O-NPS	UI/CuO-NPs	UI/Ag/Cu-NCMs	Significant
<i>Streptococcus mutans</i> ATCC 25175	10	11 ^a ± 0.28	7 ^a ± 0.28	9 ^{abc} ± 0.57	0.001
	30	11 ^a ± 1.15	7 ^a ± 1.15	9.5 ^{bc} ± 0.0	
	100	17 ^{ded} ± 1.15	11 ^a ± 0.28	14.5 ^{hijk} ± 1.15	
<i>Lactobacillus acidophilus</i> CH-2	10	9 ^a ± 0.5	7 ^a ± 0.57	7 ^a ± 0.28	0.001
	30	14 ^{db} ± 0.57	7 ^a ± 0.0	9.5 ^{cd} ± 0.28	
	100	18.3 ^{def} ± 0.57	11 ^b ± 0.57	16 ^k ± 0.57	
<i>Staphylococcus aureus</i> ATCC6538	10	10 ^a ± 0.0	7 ^a ± 0.0	7 ^a ± 0.57	0.001
	30	10 ^a ± 0.28	7 ^a ± 0.0	8 ^{ab} ± 0.57	
	100	17.5 ^{def} ± 1.15	11 ^b ± 0.57	13.5 ^{ghi} ± 0	
<i>Staphylococcus aureus</i>	10	10 ^a ± 0.57	7 ^a ± 0.0	9.5 ^{bc} ± 0.76	0.001
	30	10 ^a ± 0.0	7 ^a ± 0.0	9.5 ^{bc} ± 1.15	
	100	18.5 ^{ef} ± 0.0	17 ^d ± 0.57	13 ^{fgh} ± 1.15	
<i>Staphylococcus epidermidis</i>	10	9 ^a ± 0.28	7 ^a ± 0.0	9 ^{abc} ± 0.0	0.001
	30	11 ^a ± 0.28	8 ^a ± 0.57	10 ^{bcd} ± 0.57	
	100	19.3 ^f ± 0.57	12 ^b ± 0.57	14 ^{hij} ± 0.57	
<i>Klebsiella pneumoniae</i> KY856924	10	10 ^a ± 1.04	7 ^a ± 0.0	8 ^{ab} ± 0.86	0.001
	30	11 ^a ± 0.57	7 ^a ± 0.0	9 ^{abc} ± 0.0	
	100	16.5 ^{cd} ± 0.0	11 ^b ± 1.15	12 ^{efg} ± 0.57	
<i>Acinetobacter</i> KY856930	10	10 ^a ± 0.28	7 ^a ± 0.0	8 ^{ab} ± 0.57	0.001
	30	11 ^a ± 0.0	7 ^a ± 0.57	9 ^{abc} ± 0.28	
	100	17 ^{de} ± 1.15	10 ^b ± 1.44	13 ^{fgh} ± 1.15	
<i>E. coli</i> KY856932	10	10 ^a ± 0	7 ^a ± 0.0	8 ^{ab} ± 0.0	0.001
	30	10 ^a ± 1.15	7 ^a ± 0.0	9 ^{abc} ± 1.15	
	100	14 ^b ± 0.57	15 ^c ± 0.750.0	14 ^{hij} ± 0	

Table 4. Cont.

Bacterial Strains	Volume	UL/Ag ₂ O-NPS	UI/CuO-NPs	UI/Ag/Cu-NCMs	Significant
<i>E. coli</i> KY856933	10	11 ^a ± 0	7 ^a ± 1.15	11 ^{cde} ± 0	0.001
	30	11 ^a ± 1.05	17 ^d ± 1.44	18 ^l ± 0.57	
	100	21.3 ^g ± 0.57	20.5 ^e ± 0.0	18 ^l ± 0.0	
<i>Enterobacter</i> KY856934	10	9 ^a ± 0.57	7 ^a ± 0.0	9 ^{abc} ± 0.28	0.001
	30	17 ^{de} ± 0.28	7 ^a ± 0.0	11.5 ^{def} ± 0.0	
	100	16 ^{ab} ± 0.0	15 ^c ± 0.0	15 ^c ± 01.15	
<i>Enterobacter aerogenes</i>	10	9 ^a ± 0.28	7 ^a ± 0.57	9 ^{abc} ± 0.28	0.001
	30	10 ^a ± 0.57	7 ^a ± 1.15	9 ^{abc} ± 0	
	100	15 ^{ab} ± 0.57	14 ^c ± 0.0	15.5 ^b ± 0.57	
Sig		0.001	0.001	0.001	

Different letters in each column are significant value ($p \leq 0.05$).

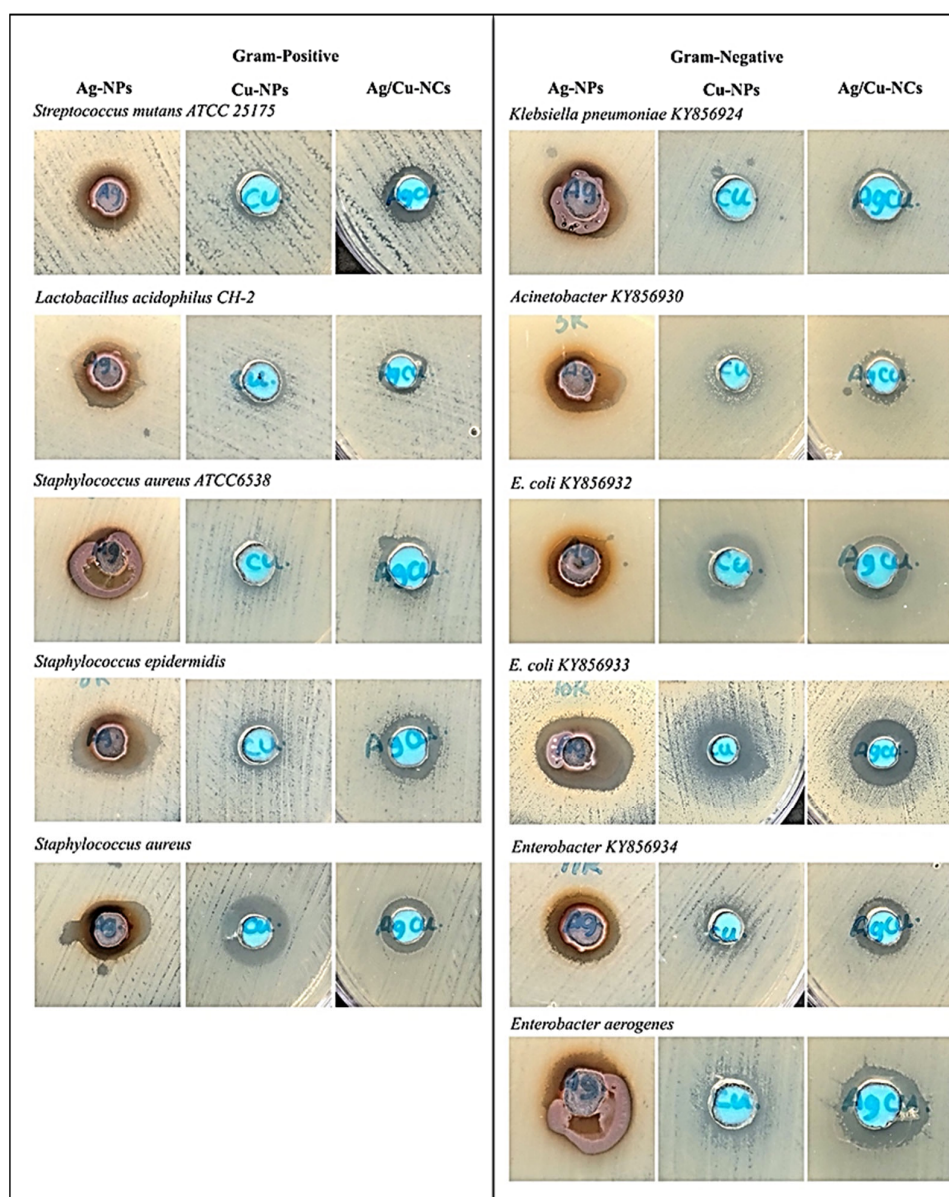


Figure 6. Antibacterial effects of green synthesized UL/Ag₂ O-NPS, UI/CuO-NPs, and UI/Ag/Cu-NCMs (100 µL/well).

Table 5. Cont.

Bacteria	Nano Types	MIC (Nano mg/mL)						MBC (Nano mg/mL)				
		1	0.5	0.25	0.125	0.062	0.03	1	0.5	0.25	0.125	0.062
<i>Staphylococcus aureus</i> ATCC 25923	UL/Ag ₂ O-NPS	–	–	–	+	+	+	–	–	–	+	+
	UI/CuO-NPs	–	–	–	+	+	+	+	+	+	+	+
	UI/Ag/Cu-NCMs	–	–	–	–	+	+	–	–	+	+	+
<i>Staphylococcus epidermidis</i> ATCC 12228	UL/Ag ₂ O-NPS	–	–	–	–	+	+	–	–	–	–	+
	UI/CuO-NPs	–	–	–	+	+	+	+	+	+	+	+
	UI/Ag/Cu-NCMs	–	–	–	–	+	+	+	+	+	+	+
<i>Klebsiella pneumoniae</i> KY856924	UL/Ag ₂ O-NPS	–	–	+	+	+	+	–	–	+	+	+
	UI/CuO-NPs	–	–	–	+	+	+	+	+	+	+	+
	UI/Ag/Cu-NCMs	–	–	–	+	+	+	+	+	+	+	+
<i>Acinetobacter</i> KY856930	UL/Ag ₂ O-NPS	–	+	+	+	+	+	–	+	+	+	+
	UI/CuO-NPs	–	–	–	+	+	+	+	+	+	+	+
	UI/Ag/Cu-NCMs	–	–	–	+	+	+	+	+	+	+	+
<i>E. coli</i> KY856932	UL/Ag ₂ O-NPS	–	–	+	+	+	+	–	–	+	+	+
	UI/CuO-NPs	–	–	–	+	+	+	+	+	+	+	+
	UI/Ag/Cu-NCMs	–	–	–	+	+	+	+	+	+	+	+
<i>E. coli</i> KY856933	UL/Ag ₂ O-NPS	–	–	–	–	–	+	–	–	–	–	+
	UI/CuO-NPs	–	–	–	+	+	+	–	–	–	+	+
	UI/Ag/Cu-NCMs	–	–	–	–	+	+	–	–	–	+	+
<i>Enterobacter</i> KY856934	UL/Ag ₂ O-NPS	–	–	–	–	–	+	–	–	–	–	+
	UI/CuO-NPs	–	–	–	+	+	+	+	+	+	+	+
	UI/Ag/Cu-NCMs	–	–	–	+	+	+	+	+	+	+	+
<i>Enterobacter aerogenes</i>	UL/Ag ₂ O-NPS	–	–	+	+	+	+	–	+	+	+	+
	UI/CuO-NPs	–	–	–	+	+	+	+	+	+	+	+
	UI/Ag/Cu-NCMs	–	–	–	+	+	+	+	+	+	+	+

Positive (+): turbidity, indicating growth; negative (–): no turbidity, indicating absence of growth.

2.4. Biofilm Formation Inhibition Assay

A static biofilm assay was performed to evaluate the effect of the synthesized UL/Ag₂ O-NPS, UI/CuO-NPs, and UI/Ag/Cu-NCMs derived from *U. lactuca* on *E. coli* KY856933 biofilm formation, and showed positive biofilm formation before treatment with the nanoparticles. Figure 7 shows the biofilm inhibition percentage at different concentrations of nanoparticles (1, 0.5, 0.25, 0.12, and 0.06 mg/mL). The results obtained in the microtiter plates show that the highest inhibition percentage was 87.02 with 0.5 mg/mL UL/Ag₂ O-NPS, followed by 1.0 mg/mL UL/Ag₂ O-NPS (86.31%). The same inhibition percentage was obtained with 0.25 mg/mL UL/Ag₂ O-NPS, and with 1.0 mg/mL UI/Ag/Cu-NCMs, the inhibition was 85.5%. The lowest percentage of biofilm inhibition was 44.38 with 0.06 mg/mL UI/CuO-NPs. The order of anti-biofilm strength formed by *Escherichia coli* ATCC 25922, *Pseudomonas aeruginosa* ATCC 27853, and *Staphylococcus aureus* ATCC 43300 with biosynthesis nanocomposite was Ag–TiO₂ > TiO₂–Ag > Cu–Ag > Ag–Cu [95]. The bio-Ag-NPs inhibited biofilm formation by both *Escherichia coli* and *S. aureus* at concentrations of 4 µg/mL [96]. The Ag-NPs demonstrated notable anti-biofilm activity against *S. aureus* biofilms and powerful bactericidal effects against *P. aeruginosa* and *S. aureus*, respectively [97]. The minimal inhibitory concentration of the produced Ag-

NPs against biofilm-forming *Staphylococcus aureus* verified their concentration-dependent inhibition (MIC) [98].

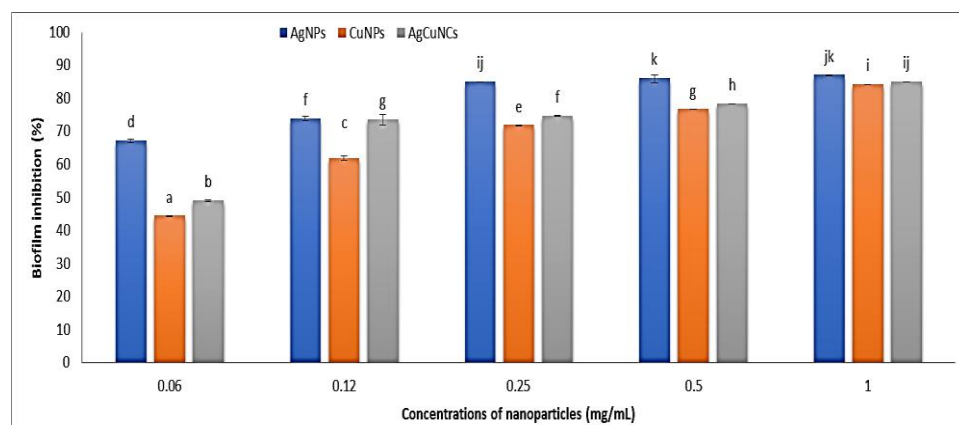


Figure 7. Anti-biofilm studies of green synthesized Ul/Ag₂ ONPS, Ul/CuO-NPs, and Ul/Ag/Cu-NCMs in the presence of biofilm-forming of *E. coli* KY856933. Different letters denote the significant values of mean; bars are St-error.

3. Material and Methods

3.1. Extraction of Algae

At the end of January, in the winter, *Ulva lactuca* (Figure 8) was gathered from the seashore (21°.637086 N and 39°.101631 E) in Jeddah, Saudi Arabia (2020). One gram of air-dried *U. lactuca* was mixed with 100 mL of deionized (D.D.) water to create the Ag-NPS and Ag–Cu NCMS. This mixture was then boiled for an hour and filtered, and the remaining 100 mL of D.D. water was added. For the CuO-NPs, 100 mL of D.D. water was combined with six grams of air-dried *U. lactuca* alga, boiled for one hour, filtered, and then the remaining 100 mL of D.D. water was added.



Figure 8. Morphological shape of *Ulva lactuca* (collected from seashore or Red Sea, Jeddah, Saudi Arabia).

3.2. Synthesis of Silver/Copper Nanocomposites (Ul/Ag/Cu-NCMs) by *U. lactuca* Extract

Briefly, 60 mL of distilled and deionized water were combined with 9 mM of copper II sulfate and 1 mM of silver nitrate (D.D. water). Drop by drop, 40 mL of aqueous algal extract was added to the Ag/Cu solution, followed by 0.2 M NaOH, which produced a grayish precipitate that was left in a magnetic stirrer for 2 h [70]. To remove the contaminants, the mixture was centrifuged, the supernatant was eliminated, and the grayish precipitate was washed twice with 50 mL of D.D. water and once more with 50 mL of ethanol by

repeated centrifugation. After one day of air drying, silver/copper nanoparticle powder was produced.

3.3. Biosynthesis of Silver Nanoparticles Using Alga Aqueous Extract

Alga extract (30 mL) was injected drop by drop with a syringe on 70 mL of 1 mM AgNO₃ on a magnetic stirrer until the color changed from clear to brown to darker brown, after ten minutes.

3.4. Biosynthesis Copper Oxide Nanoparticles (UI/CuO-NPs) by *U. lactuca* Extract

A faint blue powder of copper nanoparticles was obtained after air drying for one day. Copper II sulfate, CuSO₄ (9 mM), was added to 70 mL distal and deionized water (D.D. water) under constant stirring. Thirty ml of aqueous algal extract was added drop by drop to the copper solution. After 10 min of stirring, 0.2 M NaOH was added, changing the color from blue to greenish; this was then placed in a magnetic stirrer for 2 h [99]. The greenish precipitate was filtered and washed twice with 50 mL of D.D. water and then with 50 mL of ethanol to eliminate the impurities.

3.5. Structural and Morphological Characterization

The synthesized UL/Ag₂O-NPS, UI/Ag/Cu-NCMs, and UI/CuO-NPs were dried at 60 °C, and characterized by the following devices: scanning electron microscopy (SEM) (30 kV (SEM, JEOL JSM-6510/v, Tokyo, Japan)); transmission electron microscopy (TEM) (JEOL JSM-6510/v, Tokyo, Japan); and X-ray diffraction (XRD) (PAN Analytical X-Pert PRO, spectris plc, Almelo, The Netherlands). According to the Scherrer equation, the mean particle diameters of the nanoparticles were calculated from the XRD pattern:

$$D = K\lambda / \beta \cos\theta$$

K is constant; λ is the wavelength of the X-ray (1.54060 Å); and β is the full width at half-maximum (FWHM).

Fourier transform infrared (FTIR) spectroscopy (Thermo Fisher Nicolet IS10, (Waltham, MA, USA)), zeta potential and energy dispersion (Malvern Zeta size Nano-Zs90, Malvern, PA, USA), and X-ray spectroscopy (EDX) (JEOL JSM-6510/v, Tokyo, Japan) were also performed.

3.6. Antibacterial Assay

The antibacterial activity of UL/Ag₂O-NPS, UI/Ag/Cu-NCMs, and UI/CuO-NPs was investigated against eleven pathogenic bacterial strains. Six Gram-negative bacteria (*Klebsiella pneumoniae* KY856924, *Acinetobacter* KY856930, *E. coli* KY856932, *E. coli* KY856933, *Enterobacter* KY856934, and *Enterobacter aerogenes*), which were isolated from different medical samples and identified as multidrug-resistant in a previous study [78,100], in addition to five pathogenic Gram-positive control strains (*Klebsiella pneumoniae* KY856924, *Staphylococcus aureus* ATCC 6538, *Staphylococcus aureus* ATCC 25923, *Staphylococcus epidermidis* ATCC 12228, and *Streptococcus mutans* ATCC 25175) were utilized. All the bacterial strains were cultured in nutrient broth at 37 °C for 24 h. The bacterial strains were spread on Mueller–Hinton agar (MHA) using a sterile cotton swab. Wells were made in the agar plates and filled with 10, 30, and 100 µL of 20 mg/mL UL/Ag₂O-NPS, UI/Ag/Cu-NCMs, and UI/CuO-NPs, respectively. The plates were incubated at 37 °C for 24 h, and the zone of inhibition was observed after 24 h of incubation.

3.7. Minimum Inhibitory Concentration (MIC) Assays

The minimum inhibitory concentrations (MIC) of green synthesized nanoparticles were determined in a 24-well culture plate using standard broth micro-dilution methods to verify the antibacterial activity. Two-fold dilutions of UL/Ag₂O-NPS, UI/Ag/Cu-NCMs, and UI/CuO-NPs in concentrations ranging from 1 mg/mL to 0.062 mg/mL were prepared

to determine the MIC in the nutrient broth media. The results were observed and compared to the negative control after 24 h at 37 °C of incubation.

3.8. Minimum Bactericidal Concentration (MBC) Assays

After the MIC determination of the nanoparticles, the MBC was conducted by transferring 10 µL from each overnight MIC culture plate well to sterile Mueller–Hinton agar (MHA) fresh plates. Viable growth was determined after 24 h at 37 °C. The lowest concentration with no visible growth on the MHA plate was recorded as the MBC value.

3.9. Biofilm Formation Inhibition Assay

The biofilm inhibition assay was performed as described previously by Heikens et al. [101] and Hamed et al. [102] with the following modifications: one colony of overnight plate-grown *E. coli* KY856933 bacterial culture (which showed positive biofilm formation on Congo red agar) was resuspended in 5 mL tryptic soy broth (TSB) supplemented with 0.25% glucose on a shaking incubator at 37 °C to an OD of 660.

The bacterial cultures were diluted with fresh media (1:20) and supplemented with different concentrations (1, 0.5, 0.25, 0.12, and 0.06 mg/mL) of UL/Ag₂O-NPS, UI/CuO-NPs, and UL/Ag/Cu-NMCs separately, in addition to a culture without nanoparticles as a positive control. Then, 200 µL of each concentration was aliquoted into the wells of a 24-well flat-bottom polystyrene microtiter plate and incubated for 24 h at 37 °C without agitation. After incubation, the bacteria were removed, the wells were washed with 200 µL phosphate buffer saline (PBS), and the plates were dried for 1 h at room temperature.

A total of 100 mL of 0.2% Gram's crystal violet was added to each well for 15 min after the first hour. After the stain was eliminated, 200 µL of PBS were used to wash the plates three times. At room temperature, the plates were dried for 15 min. Each well received one milliliter of ethanol (95%) before being incubated for 15 min. At 570 nm, the reaction mixture was spectrophotometrically measured.

$$\% \text{ of inhibition} = \left(\frac{\text{OD in control} - \text{OD in treatment}}{\text{OD in control}} \right) * 100$$

3.10. Statistical Analysis

The experiments were performed in triplicate and the results were considered as the means ± standard error of the mean. An analysis of variance (ANOVA) was performed on all of the data. Duncan's multiple range tests were used to determine the significance of the variable mean differences ($p \leq 0.05$), SPSS version 16.

4. Conclusions

In this experimental study, *Ulva lactuca* aqueous extract was successfully used to synthesize silver and copper nanoparticles and their composites. Their characterization was achieved using FTIR, SEM, TEM, EDX, XRD, and the zeta potential. The FTIR analysis reveals that the functional groups of nanoparticles and their composites differ. The TEM image demonstrates changes in the shape and size of the silver and copper nanoparticles and their composites, which were biofabricated by green alga *U. lactuca*. The zeta potential denotes that the UL/Ag₂O-NPS have a positive charge, while the UI/CuO-NPs and UI/Ag/Cu-NPs have a negative charge. The fact that the UL/Ag₂O-NPS were more effective against the tested pathogenic bacteria than both the UI/CuO-NPs and UI/Ag/Cu-NPs may be due to the positive charge of UL/Ag₂O-NPS, as well as the small size of the nanoparticles. The inhibition of biofilm formation by *E. coli* KY856933 was the highest with the applied UL/Ag₂O-NPS, followed by the UI/CuO-NPs and UI/Ag/Cu-NMPs.

Author Contributions: R.A.H.: supervision, visualization, writing—review and editing. M.A.A.: methodology, writing. A.S.A. and A.M.A.: validation, resources, funding acquisition. D.A.A.: resources, funding acquisition. R.R.M.: supervision, visualization, methodology, writing, review and editing. All authors have read and agreed to the published version of the manuscript.

Funding: This research received no external funding.

Institutional Review Board Statement: Not applicable.

Informed Consent Statement: Not applicable.

Data Availability Statement: Not applicable.

Conflicts of Interest: The authors declare no conflict of interest.

Sample Availability: Samples are available upon request from R.A.H.

References

1. Shah, M.; Fawcett, D.; Sharma, S.; Tripathy, S.K.; Poinern, G.E.J. Green Synthesis of Metallic Nanoparticles via Biological Entities. *Materials* **2015**, *8*, 7278–7308. [[CrossRef](#)] [[PubMed](#)]
2. Salem, S.S.; Fouda, A. Green Synthesis of Metallic Nanoparticles and Their Prospective Biotechnological Applications: An Overview. *Biol. Trace Element Res.* **2020**, *199*, 344–370. [[CrossRef](#)] [[PubMed](#)]
3. Agrawal, K.; Gupta, V.K.; Verma, P. Microbial cell factories a new dimension in bio-nanotechnology: Exploring the robustness of nature. *Crit. Rev. Microbiol.* **2021**, *48*, 397–427. [[CrossRef](#)]
4. Prasad, R. Synthesis of Silver Nanoparticles in Photosynthetic Plants. *J. Nanopart.* **2014**, *2014*, 963961. [[CrossRef](#)]
5. Akbar, S.; Tauseef, I.; Subhan, F.; Sultana, N.; Khan, I.; Ahmed, U.; Haleem, K.S. An overview of the plant-mediated synthesis of zinc oxide nanoparticles and their antimicrobial potential. *Inorg. Nano-Metal Chem.* **2020**, *50*, 257–271. [[CrossRef](#)]
6. Purohit, J.; Chattopadhyay, A.; Singh, N.K. Green Synthesis of Microbial Nanoparticle: Approaches to Application. In *Microbial Nanobionics*; Basic Research and Applications; Springer: Berlin/Heidelberg, Germany, 2019; Volume 2, pp. 35–60. [[CrossRef](#)]
7. Manivasagan, P.; Oh, J. Marine polysaccharide-based nanomaterials as a novel source of nanobiotechnological applications. *Int. J. Biol. Macromol.* **2016**, *82*, 315–327. [[CrossRef](#)]
8. Negreanu-Pirjol, B.-S.; Negreanu-Pirjol, T.; Popoviciu, D.R.; Anton, R.-E.; Prelipcean, A.-M. Marine Bioactive Compounds Derived from Macroalgae as New Potential Players in Drug Delivery Systems: A Review. *Pharmaceutics* **2022**, *14*, 1781. [[CrossRef](#)]
9. Dahoumane, S.A.; Mechouet, M.; Wijesekera, K.; Filipe, C.D.; Sicard, C.; Bazylnski, D.A.; Jeffryes, C. Algae-mediated biosynthesis of inorganic nanomaterials as a promising route in nanobiotechnology—A review. *Green Chem.* **2017**, *19*, 552–587. [[CrossRef](#)]
10. Soni, R.A.; Rizwan, M.A.; Singh, S. Opportunities and potential of green chemistry in nanotechnology. *Nanotechnol. Environ. Eng.* **2022**, *7*, 661–673. [[CrossRef](#)]
11. Asmathunisha, N.; Kathiresan, K. A review on biosynthesis of nanoparticles by marine organisms. *Colloids Surfaces B Biointerfaces* **2013**, *103*, 283–287. [[CrossRef](#)]
12. González-Ballesteros, N.; Prado-López, S.; Rodríguez-González, J.B.; Lastra, M.; Rodríguez-Argüelles, M. Green synthesis of gold nanoparticles using brown algae *Cystoseira baccata*: Its activity in colon cancer cells. *Colloids Surf. B Biointerfaces* **2017**, *153*, 190–198. [[CrossRef](#)] [[PubMed](#)]
13. Hamouda, R.A.; Hussein, M.H.; El-Naggar, N.E.A.; Karim-Eldeen, M.A.; Alamer, K.H.; Saleh, M.A.; El-Azeem, R.M.A. Promoting effect of soluble polysaccharides extracted from *Ulva* spp. on *Zea mays* L. growth. *Molecules* **2022**, *27*, 1394. [[CrossRef](#)]
14. Dogmaz, S.; Cavas, L. Biohydrogen production via green silver nanoparticles synthesized through biomass of *Ulva lactuca* bloom. *Bioresour. Technol.* **2023**, *379*, 129028. [[CrossRef](#)]
15. Solanki, A.; Patel, G.; Hakim, M.; Patel, I. Fabrication of silver nanoparticles from marine green algal species: *Ulva lactuca* L. and *Ulva conglobata* L. and their antibacterial activity. *Med. Plants-Int. J. Phytomed. Rel. Ind.* **2023**, *15*, 194–201. [[CrossRef](#)]
16. González-Ballesteros, N.; Rodríguez-Argüelles, M.C.; Prado-López, S.; Lastra, M.; Grimaldi, M.; Cavazza, A.; Bigi, F. Macroalgae to nanoparticles: Study of *Ulva lactuca* L. role in biosynthesis of gold and silver nanoparticles and of their cytotoxicity on colon cancer cell lines. *Mater. Sci. Eng. C* **2019**, *97*, 498–509. [[CrossRef](#)] [[PubMed](#)]
17. Twardowski, T.E. *Introduction to Nanocomposite Materials: Properties, Processing, Characterization*; DEStech Publications, Inc.: Lancaster, PA, USA, 2007.
18. Mohapatra, L.; Bhattamishra, S.K.; Panigrahy, R.; Parida, S.; Pati, P. Antidiabetic Effect of *Sargassum wightii* and *Ulva fasciata* in High fat diet and Multi Low Dose Streptozotocin Induced Type 2 Diabetic Mice. *Pharm. Biosci. J.* **2016**, *4*, 13–23. [[CrossRef](#)]
19. Din, S.H.; Shah, M.A.; Sheikh, N.A.; Butt, M.M. Nano-composites and their applications: A review. *Charact. Appl. Nanomater.* **2020**, *3*, 40–48. [[CrossRef](#)]
20. Ashrafi, M.; Bayat, M.; Mortazavi, P.; Hashemi, S.J.; Meimandipour, A. Antimicrobial effect of chitosan–silver–copper nanocomposite on *Candida albicans*. *J. Nanostruct. Chem.* **2020**, *10*, 87–95. [[CrossRef](#)]
21. Mujeeb, A.A.; Khan, N.A.; Jamal, F.; Badre Alam, K.F.; Saeed, H.; Kazmi, S.; Alshameri, A.W.F.; Kashif, M.; Ghazi, I.; Owais, M. *Olax scandens* mediated biogenic synthesis of Ag–Cu nanocomposites: Potential against inhibition of drug-resistant microbes. *Front. Chem.* **2020**, *8*, 103. [[CrossRef](#)]

22. Doolotkeldieva, T.; Bobusheva, S.; Zhasnakunov, Z.; Satybaldiev, A. Biological Activity of Ag and Cu Monometallic Nanoparticles and Ag-Cu Bimetallic Nanocomposites against Plant Pathogens and Seeds. *J. Nanomater.* **2022**, *2022*, 1190280. [[CrossRef](#)]
23. Nivetha, A.; Sakthivel, C.; Hemalatha, J.; Senthamil, C.; Prabha, I. Fabrication of a bifunctionalized Calotropis gigantea inspired Ag-Cu-Co trimetal oxide for the remediation of methylene blue, and its larvicidal and antibacterial applications. *New J. Chem.* **2023**, *47*, 12375–12392. [[CrossRef](#)]
24. Sahin, F.; Camdal, A.; Demirel Sahin, G.; Ceylan, A.; Ruzi, M.; Onses, M.S. Disintegration and Machine-Learning-Assisted Identification of Bacteria on Antimicrobial and Plasmonic Ag-Cu x O Nanostructures. *ACS Appl. Mater. Interfaces* **2023**, *15*, 11563–11574. [[CrossRef](#)] [[PubMed](#)]
25. Baqir, Y.; Tunio, M.T.; Ilyas, S.Z.; Agathopoulos, S.; Mufti, H.; Jalil, A.; Hassan, A. Green synthesis and first-principles calculations of a highly efficient antibacterial agent: CuO/Ag nanocomposites. *Chem. Pap.* **2022**, *77*, 2459–2467. [[CrossRef](#)]
26. Belay, A.N.; Mihretu, M.E.; Getnet, T.G. Synthesis, characterization, and antibacterial activities of Cu-Ag bimetallic oxide nanocomposites using Eichhornia crassipes aqueous leaf extract. *J. Experim. Nanosci.* **2023**, *18*, 2202911. [[CrossRef](#)]
27. Amer, M.; Awwad, A. Green synthesis of copper nanoparticles by Citrus limon fruits extract, characterization and antibacterial activity. *Chem. Int.* **2021**, *7*, 1–8.
28. Sharma, R.; Tripathi, A. Green synthesis of nanoparticles and its key applications in various sectors. *Mater. Today Proc.* **2021**, *48*, 1626–1632. [[CrossRef](#)]
29. Krithiga, N.; Jayachitra, A.; Rajalakshmi, A. Synthesis, characterization and analysis of the effect of copper oxide nanoparticles in biological systems. *Indian J. Nat. Sci.* **2013**, *1*, 6–15.
30. Subhankari, I.; Nayak, P. Antimicrobial activity of copper nanoparticles synthesised by ginger (*Zingiber officinale*) extract. *World J. Nano Sci. Technol.* **2013**, *2*, 10–13.
31. Xu, V.W.; Nizami, M.Z.I.; Yin, I.X.; Yu, O.Y.; Lung, C.Y.K.; Chu, C.H. Application of Copper Nanoparticles in Dentistry. *Nanomaterials* **2022**, *12*, 805. [[CrossRef](#)]
32. Perelshtein, I.; Applerot, G.; Perkas, N.; Wehrschuetz-Sigl, E.; Hasmann, A.; Gübitz, G.; Gedanken, A. CuO-cotton nanocomposite: Formation, morphology, and antibacterial activity. *Surf. Coat. Technol.* **2009**, *204*, 54–57. [[CrossRef](#)]
33. Hassan, M.S.; Amna, T.; Yang, O.-B.; El-Newehy, M.H.; Al-Deyab, S.S.; Khil, M.-S. Smart copper oxide nanocrystals: Synthesis, characterization, electrochemical and potent antibacterial activity. *Coll. Surf. B Biointerfaces* **2012**, *97*, 201–206. [[CrossRef](#)] [[PubMed](#)]
34. Černik, M.; Padil, V.V.T. Green synthesis of copper oxide nanoparticles using gum karaya as a biotemplate and their antibacterial application. *Int. J. Nanomed.* **2013**, *8*, 889–898. [[CrossRef](#)] [[PubMed](#)]
35. Akhavan, O.; Ghaderi, E. Cu and CuO nanoparticles immobilized by silica thin films as antibacterial materials and photo-catalysts. *Surf. Coat. Technol.* **2010**, *205*, 219–223. [[CrossRef](#)]
36. Van Doremalen, N.; Bushmaker, T.; Morris, D.H.; Holbrook, M.G.; Gamble, A.; Williamson, B.N.; Tamin, A.; Harcourt, J.L.; Thornburg, N.J.; Gerber, S.I.; et al. Aerosol and surface stability of SARS-CoV-2 as compared with SARS-CoV-1. *New Engl. J. Med.* **2020**, *382*, 1564–1567. [[CrossRef](#)] [[PubMed](#)]
37. Daoudi, H.; Bouafia, A.; Meneceur, S.; Laouini, S.E.; Belkhalifa, H.; Lebhihi, R.; Selmi, B. Secondary Metabolite from Nigella Sativa Seeds Mediated Synthesis of Silver Oxide Nanoparticles for Efficient Antioxidant and Antibacterial Activity. *J. Inorg. Organomet. Polym. Mater.* **2022**, *32*, 4223–4236. [[CrossRef](#)]
38. Watanabe, T.; Ebata, T.; Tanabe, S.; Mikami, N. Size-selected vibrational spectra of phenol-(H₂O)_n (n = 1–4) clusters observed by IR-UV double resonance and stimulated Raman-UV double resonance spectroscopies. *J. Chem. Phys.* **1996**, *105*, 408–419. [[CrossRef](#)]
39. Mossoba, M.M.; Al-Khaldi, S.F.; Kirkwood, J.; Fry, F.S.; Sedman, J.; Ismail, A.A. Printing microarrays of bacteria for identification by infrared microspectroscopy. *Vibrat. Spectr.* **2005**, *38*, 229–235. [[CrossRef](#)]
40. Lingegowda, D.C.; Kumar, J.K.; Prasad, A.D.; Zarei, M.; Gopal, S. FTIR spectroscopic studies on cleome gynandra-Comparative analysis of functional group before and after extraction. *Rom. J. Biophys.* **2012**, *22*, 137–143.
41. Popova, A.; Christov, M.; Raicheva, S.; Sokolova, E. Adsorption and inhibitive properties of benzimidazole derivatives in acid mild steel corrosion. *Corros. Sci.* **2004**, *46*, 1333–1350. [[CrossRef](#)]
42. Munir, M.; Shahid, M.; Munir, H.; Javaid, S.; Sharif, S.; El-Ghorab, A.; El-Ghorab, A. Xanthan gum biochemical profiling, anti-oxidant, antibacterial, biofilm inhibition and mutagenic potential. *Curr. Sci.* **2017**, *114*, 1903–1913.
43. Rangel-Vazquez, N.A.; Sánchez-López, C.; Felix, F.R. Spectroscopy analyses of polyurethane/polyaniline IPN using computational simulation (Amber, MM+ and PM3 method). *Polímeros* **2014**, *24*, 453–463. [[CrossRef](#)]
44. Lima, C.A.; Goulart, V.P.; Correa, L.; Pereira, T.M.; Zezell, D.M. ATR-FTIR spectroscopy for the assessment of biochemical changes in skin due to cutaneous squamous cell carcinoma. *Int. J. Mol. Sci.* **2015**, *16*, 6621–6630. [[CrossRef](#)] [[PubMed](#)]
45. Samargandi, D.; Zhang, X.; Liu, F.; Tian, S. Fourier Transform Infrared (FT-IR) spectroscopy for discrimination of fenugreek seeds from different producing areas. *J. Chem. Pharm. Res.* **2014**, *6*, 19–24.
46. Devi, T.R.; Gayathri, S. FTIR and FT-Raman spectral analysis of paclitaxel drugs. *Int. J. Pharm. Sci. Rev. Res.* **2010**, *2*, 106–110.
47. Verdonck, M.; Denayer, A.; Delvaux, B.; Garaud, S.; De Wind, R.; Desmedt, C.; Sotiriou, C.; Willard-Gallo, K.; Goormaghtigh, E. Characterization of human breast cancer tissues by infrared imaging. *Analyst* **2015**, *141*, 606–619. [[CrossRef](#)]
48. Dovbeshko, G.I.; Gridina, N.Y.; Kruglova, E.B.; Pashchuk, O.P. FTIR spectroscopy studies of nucleic acid damage. *Talanta* **2000**, *53*, 233–246. [[CrossRef](#)]

49. Dukor, R.K. Vibrational Spectroscopy in the Detection of Cancer. In *Handbook of Vibrational Spectroscopy*; John Wiley & Sons: Hoboken, NJ, USA, 2006. [\[CrossRef\]](#)
50. Wood, B.R.; Quinn, M.A.; Tait, B.; Ashdown, M.; Hislop, T.; Romeo, M.; McNaughton, D. FTIR microspectroscopic study of cell types and potential confounding variables in screening for cervical malignancies. *Biospectroscopy* **1998**, *4*, 75–91. [\[CrossRef\]](#)
51. Gilardoni, S.; Liu, S.; Takahama, S.; Russell, L.M.; Allan, J.D.; Steinbrecher, R.; Jimenez, J.L.; De Carlo, P.F.; Dunlea, E.J.; Baumgardner, D. Characterization of organic ambient aerosol during MIRAGE 2006 on three platforms. *Atmos. Meas. Tech.* **2009**, *9*, 5417–5432. [\[CrossRef\]](#)
52. Das, D.D.; Schnitzer, M.I.; Monreal, C.M.; Mayer, P. Chemical composition of acid–base fractions separated from bio-oil derived by fast pyrolysis of chicken manure. *Bioresour. Technol.* **2009**, *100*, 6524–6532. [\[CrossRef\]](#)
53. Li, X.; Lin, J.; Ding, J.; Wang, S.; Liu, Q.; Qing, S. Raman spectroscopy and fluorescence for the detection of liver cancer and abnormal liver tissue. In Proceedings of the 26th Annual International Conference of the IEEE Engineering in Medicine and Biology Society, San Francisco, CA, USA, 1–5 September 2004; pp. 212–215.
54. Ahmed, Y.M.Z.; El-Sheikh, S.M.; Zaki, Z.I. Changes in hydroxyapatite powder properties via heat treatment. *Bull. Mater. Sci.* **2015**, *38*, 1807–1819. [\[CrossRef\]](#)
55. El Bialy, B.E.; Hamouda, R.A.; Abd Eldaim, M.A.; El Ballal, S.S.; Heikal, H.S.; Khalifa, H.K.; Hozzein, W.N. Comparative toxicological effects of biologically and chemically synthesized copper oxide nanoparticles on mice. *Int. J. Nano-Med.* **2020**, *15*, 3827–3842. [\[CrossRef\]](#) [\[PubMed\]](#)
56. Ismail, M.; Khan, S.A.; Qayum, M.; Khan, M.A.; Anwar, Y.; Akhtar, K.; Asiri, A.M.; Khan, S.B. Green synthesis of antibacterial bimetallic Ag–Cu nanoparticles for catalytic reduction of persistent organic pollutants. *J. Mater. Sci. Mater. Electron.* **2018**, *29*, 20840–20855. [\[CrossRef\]](#)
57. Esmaeil Lashgarian, H.; Karkhane, M.; Kamil Alhameedawi, A.; Marzban, A. Phyco-Mediated Synthesis of Ag/AgCl Nanoparticles Using Ethanol Extract of a Marine Green Algae, *Ulva fasciata* Delile with Biological Activity. *Biointerface Res. Appl. Chem.* **2021**, *11*, 14545–14554.
58. Govindaraju, K.; Kiruthiga, V.; Kumar, V.G.; Singaravelu, G. Extracellular Synthesis of Silver Nanoparticles by a Marine Alga, *Sargassum Wightii* Grevilli and Their Antibacterial Effects. *J. Nanosci. Nanotechnol.* **2009**, *9*, 5497–5501. [\[CrossRef\]](#) [\[PubMed\]](#)
59. Rajeshkumar, S.; Kannan, C.; Annadurai, G. Synthesis and characterization of antimicrobial silver nanoparticles using marine brown seaweed *Padina tetrastrum*. *Drug Invent Today* **2012**, *4*, 511–513.
60. Kumar, P.; Selvi, S.S.; Govindaraju, M. Seaweed-mediated biosynthesis of silver nanoparticles using *Gracilaria corticata* for its antifungal activity against *Candida* spp. *Appl. Nanosci.* **2013**, *3*, 495–500. [\[CrossRef\]](#)
61. Varghese, B.; Kurian, M.; Krishna, S.; Athira, T. Biochemical synthesis of copper nanoparticles using *Zingiber officinalis* and *Curcuma longa*: Characterization and antibacterial activity study. *Mater. Today Proc.* **2020**, *25*, 302–306. [\[CrossRef\]](#)
62. Iliger, K.S.; Sofi, T.A.; Bhat, N.A.; Ahanger, F.A.; Sekhar, J.C.; Elhendi, A.Z.; Al-Huqail, A.A.; Khan, F. Copper nanoparticles: Green synthesis and managing fruit rot disease of chilli caused by *Colletotrichum capsici*. *Saudi J. Biol. Sci.* **2020**, *28*, 1477–1486. [\[CrossRef\]](#)
63. Ijaz, F.; Shahid, S.; Khan, S.A.; Ahmad, W.; Zaman, S. Green synthesis of copper oxide nanoparticles using *Abutilon indicum* leaf extract: Antimicrobial, antioxidant and photocatalytic dye degradation activities. *Trop. J. Pharm. Res.* **2017**, *16*, 743. [\[CrossRef\]](#)
64. Ramzan, M.; Obodo, R.; Mukhtar, S.; Ilyas, S.; Aziz, F.; Thovhogi, N. Green synthesis of copper oxide nanoparticles using *Cedrus deodara* aqueous extract for antibacterial activity. *Mater. Today Proc.* **2020**, *36*, 576–581. [\[CrossRef\]](#)
65. Amaliyah, S.; Pangesti, D.P.; Masruri, M.; Sabarudin, A.; Sumitro, S.B. Green synthesis and characterization of copper nanoparticles using Piper retrofractum Vahl extract as bioreductor and capping agent. *Heliyon* **2020**, *6*, e04636. [\[CrossRef\]](#) [\[PubMed\]](#)
66. Mahmoud, A.E.D.; Al-Qahtani, K.M.; Alflaj, S.O.; Al-Qahtani, S.F.; Alsamhan, F.A. Green copper oxide nanoparticles for lead, nickel, and cadmium removal from contaminated water. *Sci. Rep.* **2021**, *11*, 12547. [\[CrossRef\]](#) [\[PubMed\]](#)
67. Pol, V.G.; Grisar, H.; Gedanken, A. Coating noble metal nanocrystals (Ag, Au, Pd, and Pt) on polystyrene spheres via ultrasound irradiation. *Langmuir* **2005**, *21*, 3635–3640. [\[CrossRef\]](#) [\[PubMed\]](#)
68. López-Ubaldo, F.; Sánchez-Mendieta, V.; Olea-Mejía, O.F.; María, S.G.-P.; Luckie, R.A.M. Biosynthesis of Ag/Cu bimetallic nanoparticles using *Ricinus communis* and their antibacterial and antifungal activity. *Adv. Nat. Sci. Nanosci. Nanotechnol.* **2020**, *11*, 025018. [\[CrossRef\]](#)
69. Rocha-Rocha, O.; Cortez-Valadez, M.; Hernández-Martínez, A.R.; Gámez-Corrales, R.; Alvarez, R.A.B.; Britto-Hurtado, R.; Delgado-Beleño, Y.; Martínez-Nuñez, C.E.; Pérez-Rodríguez, A.; Arizpe-Chávez, H.; et al. Green Synthesis of Ag-Cu Nanoalloys Using *Opuntia ficus-indica*. *J. Electron. Mater.* **2016**, *46*, 802–807. [\[CrossRef\]](#)
70. Mohamad, N.; Arham, N.; Junaidah, J.; Hadi, A.; Idris, S. Green Synthesis of Ag, Cu and AgCu Nanoparticles using Palm Leaves Extract as the Reducing and Stabilizing Agents. In *IOP Conference Series: Materials Science and Engineering*; IOP Publishing: Bristol, UK, 2018; p. 012063.
71. Ginting, B.; Maulana, I.; Karnila, I. Biosynthesis Copper Nanoparticles using *Blumea balsamifera* Leaf Extracts: Characterization of its Antioxidant and Cytotoxicity Activities. *Surf. Interfaces* **2020**, *21*, 100799. [\[CrossRef\]](#)
72. Abdellatif, K.F.; Abdelfattah, R.H.; El-Ansary, M.S.M. Green Nanoparticles Engineering on Root-knot Nematode Infecting Eggplants and Their Effect on Plant DNA Modification. *Iran. J. Biotechnol.* **2016**, *14*, 250–259. [\[CrossRef\]](#)
73. Hamouda, R.A.; Yousuf, W.E.; Abdeen, E.E.; Mohamed, A. Biological and chemical synthesis of silver nanoparticles: Characterization, MIC and antibacterial activity against pathogenic bacteria. *J. Chem. Pharm. Res.* **2019**, *11*, 1–12.

74. Abo-Elmagd, R.A.; Hamouda, R.A.; Hussein, M.H. Phycotoxicity and catalytic reduction activity of green synthesized Oscillatoria gelatin-capped silver nanoparticles. *Sci. Rep.* **2022**, *12*, 20378. [[CrossRef](#)]
75. Aboeita, N.M.; Fahmy, S.A.; El-Sayed, M.M.H.; Azzazy, H.M.E.-S.; Shoeib, T. Enhanced Anticancer Activity of Nedaplatin Loaded onto Copper Nanoparticles Synthesized Using Red Algae. *Pharmaceutics* **2022**, *14*, 418. [[CrossRef](#)]
76. Marzban, A.; Mirzaei, S.Z.; Karkhane, M.; Ghotekar, S.K.; Danesh, A. Biogenesis of copper nanoparticles assisted with seaweed polysaccharide with antibacterial and antibiofilm properties against methicillin-resistant *Staphylococcus aureus*. *J. Drug Deliv. Sci. Technol.* **2022**, *74*, 103499. [[CrossRef](#)]
77. Fayaz, A.M.; Balaji, K.; Girilal, M.; Yadav, R.; Kalachelvan, P.T.; Venketesan, R. Biogenic synthesis of silver nanoparticles and their synergistic effect with antibiotics: A study against gram-positive and gram-negative bacteria. *Nanomed. Nanotechnol. Biol. Med.* **2010**, *6*, 103–109. [[CrossRef](#)]
78. Elgamily, H.; Safy, R.; Makharia, R. Influence of Medicinal Plant Extracts on the Growth of Oral Pathogens *Streptococcus Mutans* and *Lactobacillus Acidophilus*: An In-Vitro Study. *Open Access Maced. J. Med. Sci.* **2019**, *7*, 2328–2334. [[CrossRef](#)] [[PubMed](#)]
79. Abo-Elmagd, R.A.; Hussein, M.H.; Hamouda, R.A.; Shalan, A.E.; Abdelrazak, A. Statistical optimization of photo-induced biofabrication of silver nanoparticles using the cell extract of *Oscillatoria limnetica*: Insight on characterization and antioxidant potentiality. *RSC Adv.* **2020**, *10*, 44232–44246. [[CrossRef](#)] [[PubMed](#)]
80. Abbaszadegan, A.; Ghahramani, Y.; Gholami, A.; Hemmateenejad, B.; Dorostkar, S.; Nabavizadeh, M.; Sharghi, H. The effect of charge at the surface of silver nanoparticles on antimicrobial activity against gram-positive and gram-negative bacteria: A pre-liminary study. *J. Nanomater.* **2015**, *16*, 53. [[CrossRef](#)]
81. El Badawy, A.M.; Silva, R.G.; Morris, B.; Scheckel, K.G.; Suidan, M.T.; Tolaymat, T.M. Surface Charge-Dependent Toxicity of Silver Nanoparticles. *Environ. Sci. Technol.* **2010**, *45*, 283–287. [[CrossRef](#)]
82. Franci, G.; Falanga, A.; Galdiero, S.; Palomba, L.; Rai, M.; Morelli, G.; Galdiero, M. Silver Nanoparticles as Potential Antibacterial Agents. *Molecules* **2015**, *20*, 8856–8874. [[CrossRef](#)]
83. Gu, H.; Chen, X.; Chen, F.; Zhou, X.; Parsaee, Z. Ultrasound-assisted biosynthesis of CuO-NPs using brown alga *Cystoseira trinodis*: Characterization, photocatalytic AOP, DPPH scavenging and antibacterial investigations. *Ultrason. Sonochem.* **2018**, *41*, 109–119. [[CrossRef](#)]
84. Chandraker, S.K.; Lal, M.; Ghosh, M.K.; Tiwari, V.; Ghorai, T.K.; Shukla, R. Green synthesis of copper nanoparticles using leaf extract of *Ageratum houstonianum* Mill. and study of their photocatalytic and antibacterial activities. *Nano Express* **2020**, *1*, 010033. [[CrossRef](#)]
85. Jayarambabu, N.; Akshaykranth, A.; Rao, T.V.; Rao, K.V.; Kumar, R.R. Green synthesis of Cu nanoparticles using *Curcuma longa* extract and their application in antimicrobial activity. *Mater. Lett.* **2019**, *259*, 126813. [[CrossRef](#)]
86. Jayandran, M.; Haneefa, M.; Balasubramanian, V. Green synthesis and characterization of Manganese nanoparticles using natural plant extracts and its evaluation of antimicrobial activity. *J. Appl. Pharm. Sci.* **2015**, *5*, 105–110. [[CrossRef](#)]
87. Yousaf, H.; Mehmood, A.; Ahmad, K.S.; Raffi, M. Green synthesis of silver nanoparticles and their applications as an alter-native antibacterial and antioxidant agents. *Mater. Sci. Eng. C* **2020**, *112*, 110901. [[CrossRef](#)] [[PubMed](#)]
88. Panpaliya, N.P.; Dahake, P.T.; Kale, Y.J.; Dadpe, M.V.; Kendre, S.B.; Siddiqi, A.G.; Maggavi, U.R. In vitro evaluation of antimicrobial property of silver nanoparticles and chlorhexidine against five different oral pathogenic bacteria. *Saudi Dent. J.* **2019**, *31*, 76–83. [[CrossRef](#)] [[PubMed](#)]
89. Tamayo, L.A.; Zapata, P.A.; Vejar, N.D.; Azócar, M.I.; Gulppi, M.A.; Zhou, X.; Thompson, G.E.; Rabagliati, F.M.; Páez, M.A. Release of silver and copper nanoparticles from polyethylene nanocomposites and their penetration into *Listeria monocytogenes*. *Mater. Sci. Eng. C* **2014**, *40*, 24–31. [[CrossRef](#)] [[PubMed](#)]
90. Rather, R.A.; Sarwara, R.K.; Das, N.; Pal, B. Impact of reducing and capping agents on carbohydrates for the growth of Ag and Cu nanostructures and their antibacterial activities. *Particuology* **2019**, *43*, 219–226. [[CrossRef](#)]
91. Tao, Y.; Zhou, F.; Wang, K.; Yang, D.; Sacher, E. AgCu NP Formation by the Ag NP Catalysis of Cu Ions at Room Temperature and Their Antibacterial Efficacy: A Kinetic Study. *Molecules* **2022**, *27*, 6951. [[CrossRef](#)]
92. Mukherji, S.; Ruparelia, J.; Agnihotri, S. Antimicrobial Activity of Silver and Copper Nanoparticles: Variation in Sensitivity Across Various Strains of Bacteria and Fungi. In *Nano-Antimicrobials*; Springer: Berlin/Heidelberg, Germany, 2011; pp. 225–251. [[CrossRef](#)]
93. Fellahi, O.; Sarma, R.K.; Das, M.R.; Saikia, R.; Marcon, L.; Coffinier, Y.; Hadjersi, T.; Maamache, M.; Boukherroub, R. The antimicrobial effect of silicon nanowires decorated with silver and copper nanoparticles. *Nanotechnology* **2013**, *24*, 495101. [[CrossRef](#)]
94. Ruparelia, J.P.; Chatterjee, A.K.; Duttgupta, S.P.; Mukherji, S. Strain specificity in antimicrobial activity of silver and copper nanoparticles. *Acta Biomater.* **2008**, *4*, 707–716. [[CrossRef](#)]
95. Rtimi, S.; Sanjines, R.; Pulgarin, C.; Kiwi, J. Microstructure of Cu–Ag uniform nanoparticulate films on polyurethane 3D catheters: Surface properties. *ACS Appl. Mater. Interfaces* **2016**, *8*, 56–63. [[CrossRef](#)]
96. Alavi, M.; Karimi, N. Antiplanktonic, antibiofilm, antismearing motility and anti-quorum sensing activities of green synthesized Ag–TiO₂, TiO₂–Ag, Ag–Cu and Cu–Ag nanocomposites against multi-drug-resistant bacteria. *Artif. Cells Nanomed. Biotechnol.* **2018**, *46* (Suppl. 3), 399–413. [[CrossRef](#)]

97. Das, B.; Dash, S.K.; Mandal, D.; Ghosh, T.; Chattopadhyay, S.; Tripathy, S.; Das, S.; Dey, S.K.; Das, D.; Roy, S. Green synthesized silver nanoparticles destroy multidrug resistant bacteria via reactive oxygen species mediated membrane damage. *Arab. J. Chem.* **2017**, *10*, 862–876. [[CrossRef](#)]
98. Shakhathreh, M.A.; Al-Rawi, O.F.; Swedan, S.F.; Alzoubi, K.H.; Khabour, O.F.; Al-Fandi, M. Biosynthesis of silver nanoparticles from *Citrobacter freundii* as antibiofilm agents with their cytotoxic effects on human cells. *Curr. Pharm. Biotechnol.* **2021**, *22*, 1254–1263. [[CrossRef](#)] [[PubMed](#)]
99. El-Saadony, M.T.; El-Hack, M.E.A.; Taha, A.E.; Fouda, M.M.G.; Ajarem, J.S.; Maodaa, S.N.; Allam, A.A.; Elshaer, N. Ecofriendly Synthesis and Insecticidal Application of Copper Nanoparticles against the Storage Pest *Tribolium castaneum*. *Nanomaterials* **2020**, *10*, 587. [[CrossRef](#)] [[PubMed](#)]
100. Makharitha, R.R.; El-Kholy, I.; Hetta, H.F.; Abdelaziz, M.H.; Hagagy, F.I.; Ahmed, A.A.; Algammal, A.M. Antibiofilm and genetic characterization of carbapenem-resistant gram-negative pathogens incriminated in healthcare-associated infections. *Infect. Drug Resist.* **2020**, *4*, 3991–4002. [[CrossRef](#)]
101. Heikens, E.; Bonten, M.J.M.; Willems, R.J.L. Enterococcal Surface Protein Esp Is Important for Biofilm Formation of *Enterococcus faecium* E1162. *J. Bacteriol.* **2007**, *189*, 8233–8240. [[CrossRef](#)]
102. Hamed, A.; Abdel-Razek, A.S.; Araby, M.; Abu-Elghait, M.; El-Hosari, D.G.; Frese, M.; Soliman, H.S.M.; Stammmler, H.G.; Sewald, N.; Shaaban, M. Meleagrin from marine fungus *Emericella dentata* Nq45: Crystal structure and diverse biological activity studies. *Nat. Prod. Res.* **2021**, *35*, 3830–3838. [[CrossRef](#)]

Disclaimer/Publisher’s Note: The statements, opinions and data contained in all publications are solely those of the individual author(s) and contributor(s) and not of MDPI and/or the editor(s). MDPI and/or the editor(s) disclaim responsibility for any injury to people or property resulting from any ideas, methods, instructions or products referred to in the content.